Electronic Supplementary Material (ESI) for Dalton Transactions.
This journal is © The Royal Society of Chemistry 2021

Supporting information

Towards rainbow photo/electro-luminescence in copper(I) complexes with the versatile bridged bis-pyridyl ancillary ligand

Gilbert Umuhire Mahoro,[ab]† Elisa Fresta,[c]† Margaux Elie,[a] Davide di Nasso,[a] Qi Zhang,[fg] Jean-François Lohier,[a] Jean-Luc Renaud,[a] Mathieu Linares,[de] Reinhold Wannemacher,[f] Juan Cabanillas-Gonzalez,[f] Rubén D. Costa*[c] and Sylvain Gaillard*[a]

- *a. Normandie Univ, ENSICAEN, UNICAEN, CNRS, LCMT, 14000 Caen, France. E-mail: sylvain.gaillard@ensicaen.fr.*
- *b. Universidad Autónoma de Madrid, Departamento de Física Aplicada, Calle Francisco Tomás y Valiente, 7, 28049 Madrid, Spain.*
- *c. Technical University of Munich, Chair of Biogenic Functional Materials, Schulgasse 22, 94315 Straubing, Germany. ruben.costa@tum.de*
- *d. Laboratory of Organic Electronics and Group of Scientific Visualization, ITN, Linköping University,60174 Norrköping, Sweden*
- *e. Swedish e-Science Reseach Center (SeRC), Linkoping University, 58183 Linköping, Sweden*
- *f. IMDEA Nanociencia, Calle Faraday 9, Ciudad Universitaria de Cantoblanco, 28049, Madrid, Spain.*
- *g. Physical Science and Engineering Division (PSE), King Abdullah, University of Science and Technology (KAUST), 23955-6900, Thuwal, Saudi Arabia*

† These authors contributed equally

Table of content

Synthesis and NMR spectra……………………………………………………………………………………..……S3

Determination of the weak interactions in complexes **1**-**7**……………………….…………………S24

Cyclic Voltammetry of complexes **1**-**7**……………………………………………………………………….S29

Theoretically and experimentally photophysical characterization…………………………..……S32

Device characterization………………………………………………………………………………………….S39

Thin film morphologies prepared with complexes **1**-**7**….……………………………………………S42

References……………………………………………………………………….…………………………………….S44

Synthesis and NMR spectra

General considerations

Synthesis: All commercial compounds were purchased from chemical suppliers and were used as received unless stated otherwise. All reactions were carried out using standard Schleck technique. All air and water sensitive reactions were carried out under dry argon atmosphere. Solvents were purchased from Carlo Erba and degassed prior to their use by bubbling argon gas directly in the solvent. NMR spectra were recorded at room temperature on 400 MHz, 500 MHz and 600 MHz Brücker spectrometers at 298 K unless stated otherwise. Proton (^{1}H) NMR information is given in the following format: multiplicity (s, singlet; d, doublet; t, triplet; q, quartet; quin, quintet; sex, sextet; sept, septet; m, multiplet), coupling constant(s) (*J*) in Hertz (Hz), number of protons. The prefix app is occasionally applied when the lower-lying signal multiplicity was unresolved and *br* indicates the signal in question is broadened. Carbon (^{13}C) NMR spectra are reported in ppm (δ) relative to residual $CDCl_3$ (δ 77.0) unless stated otherwise. Fluor (^{19}F) and Phosphorus (^{31}P) are also reported in ppm. HRMS were performed by LCMT analytical services. **L2** was commercially available and purchased from Sigma-Aldrich.

Synthesis of the ligands

2,2'-(Propane-2,2-diyl)dipyridine L1. To a solution of di(pyridin-2-yl) methane (170 mg, 1.00 mmol) in dry degassed THF (0.3 M) at -78 °C under argon atmosphere was added dropwise a solution of *n*-butyllithium in hexane 2.5 M (440 µL, 1.10 mmol), followed by methyl iodide (75 µL, 1.20 mmol). After 1 h at -78˚C, a 2.5 M solution of n-butyllithium in hexane 2.5 M (440 µL, 1.10 mmol) was added dropwise. The reaction mixture was kept at -78 °C for 1 h and methyl iodide (187 µL, 3 mmol) was added dropwise at -78 °C, the reaction mixture was kept at -78˚C for another 2 h then the mixture was brought to room temperature and stirred overnight. The reaction was quenched at 0 °C by the addition of a saturated solution of ammonium chloride (2 mL). THF was evaporated and the aqueous layer was extracted with ethyl acetate (3x2 mL). The combined organic layers were washed with a saturated solution of Na_2CO_3 (3 mL) and brine (3 mL), dried over $MgSO_4$ and concentrated *in vacuo*. Purification by flash column chromatography (Pentane/EA) afforded an off-white solid (98 mg, 0.50 mmol, 50%). **^{1}H NMR (400 MHz, $CDCl_3$)** δ_H: 8.58 – 8.53 (*br* d, *J* = 4.0 Hz, 2H), 7.58 (dt, *J* = 7.7, 1.9 Hz, 2H), 7.21 – 7.16 (*br* d, *J* = 8.0 Hz, 2H), 7.09 (ddd, *J* = 7.4, 4.9, 1.1 Hz, 2H), 1.81 (s, 6H) ppm. In good agreement with the literature.[1]

2,2'-Oxydipyridine L3. To a mixture of CuI (95.2 mg, 0.50 mmol), K_3PO_4 (3.18 g, 15 mmol) and 2-bromopyridine (494 µL, 0.5 mmol) in degassed absolute ethanol (1 M) under argon atmosphere was added 2,2,6,6-tetramethylheptane-3,5-dione (313 µL, 1.50 mmol) and degassed distilled water (1 M). After 32 h at 130 ˚C, the reaction mixture was cooled down to room temperature, the organic layer was extracted with CH_2Cl_2 (3x15 mL), dried over $MgSO_4$, filtered and concentrated *in vacuo*. Purification by flash column chromatography (pentane/ethyl acetate/Et_3N 6/3/1) afforded a dark green oil 220 mg, 1.28 mmol, 51%. **^{1}H NMR (500 MHz, $CDCl_3$)** δ_H: 8.80 – 8.20 (*br* s, 2H), 7.79 (t, 2H), 7.27 – 7.10 (*br* s, 4H) ppm. In good agreement with the literature.[2]

2,2'-(Phenylphosphanediyl)dipyridine L4. To a solution of 2.5 M butyllithium in hexane (5 mL, 12.5 mmol) at -78 ˚C was added a solution of 2-bromopyridine (2.00 g, 12.6 mmol) in dry Et_2O (5 mL). After 4 h at -78˚C, a solution of *P,P*-dichlorophenylphosphine (860 µL, 6.25 mmol) in dry Et_2O (8 mL) was added dropwise and the reaction mixture was kept at -78˚C for 2 h, then brought to room temperature and extracted with a solution of 2 M H_2SO_4 (2x20 mL). The acidic layer was neutralized dropwise with a saturated solution of NaOH, affording a precipitate which was collected on a frit, washed with water and pentane and dried *in vacuo*. The product was obtained as a yellow solid (1.20 g, 4.50 mmol, 72% yield). **^{1}H NMR (400 MHz, $CDCl_3$)** δ_H: 8.72 (d, *J* = 4.9 Hz, 2H), 7.58 (tt, *J* = 7.7, 1.7 Hz, 2H), 7.53 – 7.47

(m, 2H), 7.41 – 7.35 (m, 3H), 7.24 (ddd, *J* = 7.9, 2,2, 1.3 Hz, 2H), 7.08 – 7.03 (ddt, 7.6, 4.9, 1.3 Hz, 2H) ppm. **^{31}P NMR (162 MHz, $CDCl_3$)** δ_P: -2.76 (s, 1P) ppm. In good agreement with the literature.[3]

2,2′-Di(pyridin-2-yl)sulfane L6. To a solution of KOH (2 equiv) in dry DMSO (0.5 M) under argon atmosphere was added pyridine-2-thiol (500 mg, 4.50 mmol, 1 equiv) followed by the addition of 2-bromopyridine (530µL, 5.40 mmol, 1.2 equiv). After 4 h at 140 ˚C, the reaction was cooled down to R.T., a saturated solution of KCl (100 mL) was added, the organic layer was extracted with CH_2Cl_2 (3x100 mL), combined, washed with a saturated solution of KCl (300 mL), filtered, concentrated *in vacuo*.[4] Purification by flash column chromatography (pentane/ethyl acetate/Et_3N: 5/4/1) afforded a colorless oil. (730 mg, 3.88 mmol, 86%). **^{1}H NMR (500 MHz, $CDCl_3$)** δ_H: 8.57 – 8.53 (*br* d, *J* = 4.6 Hz, 2H), 7.63 (dt, *J* = 7.7, 1.9 Hz, 2H), 7.47 – 7.43 (*br* d, *J* = 7.8 Hz, 2H), 7.17 (ddd, *J* = 7.3, 4.7, 1.1 Hz, 2H) ppm. In good agreement with the literature.[5]

2,2′-Dipyridylsulfone L7. To a solution of di(pyridin-2-yl)sulfane (376 mg, 2.00 mmol) and $RuCl_3$ (320 µg, 0.02 mol) in a 1:1:2 ratio of CH_3CN:CCl_4:H_2O (0.25 M) were added $NaIO_4$ (1.06 g, 5 mmol). After 12 h at room temperature, the reaction mixture was neutralized with a saturated solution of $NaHCO_3$, filtered and washed with ethyl acetate. The filtrate mixture was extracted with ethyl acetate (3x20 mL) then the organic layers were combined, dried over $MgSO_4$, filtered and concentrated *in vacuo*.[6] Purification by flash column chromatography (cyclohexane/ethyl acetate: 4.5/5.5) afforded a white powder (238 mg, 1.08 mmol, 54%). **^{1}H NMR (DMSO-*d_6*, 500 MHz)** δ_H: 8.70 – 8.66 (d, *J* = 4.4 Hz, 2H), 8.28 (d, *J* = 7.8 Hz, 2H), 8.20 (dt, *J* = 7.6, 1.6 Hz, 2H), 7.73 (ddd, *J* = 7.7, 4.7, 0.8 Hz, 2H) ppm. In good agreement with the literature.[7]

Synthesis of the Complexes

General procedure: A solution of $[Cu(CH_3CN)_4][PF_6]$ (1 equiv) and POP (1 equiv) in dry and degassed CH_2Cl_2 (0.01 M) under argon was stirred for 1 h at room temperature, then N^N ligand (1 equiv) was added. The mixture was then filtered through Celite®, concentrated *in vacuo*. The residue was dissolved in a minimum of CH_2Cl_2 then precipitated by the addition of pentane and ether. The precipitate was washed by pentane and ether. The pure product was afforded by recrystallization in acetone/ CH_2Cl_2/diethyl ether/pentane.

Copper(I) [2-(2-diphenylphosphanylphenoxy)phenyl]-diphenylphosphane; 2,2′-dipyridylamine] hexafluorophosphate Complex 2: Following the general procedure from 0.50 mmol, Yield: 445 mg, 0.48 mmol, 97%. **^{1}H NMR (500 MHz, Acetone-*d_6*)** δ_H: 9.50 (s, 1H, NH), 7.97 (d, *J* = 4.5 Hz, 2H), 7.71 (t, *J* = 7.8 Hz, 2H), 7.42 – 7.35 (m, 6H), 7.30 (t, *J* = 7.4 Hz, 8H), 7.24 – 7.17 (m, 8H), 7.15 – 7.09 (m, 6H), 6.90 – 6.84 (m, 2H), 6.70 (t, *J* = 6.3 Hz, 2H) ppm. In good agreement with the literature.[8]

Copper(I) [2-(2-diphenylphosphanylphenoxy)phenyl]-diphenylphosphane, 2,2′-di(pyridin-2-yl)sulfane] hexafluorophosphate Complex 6. Following the general procedure from 0.51 mmol, Yield: 417 mg, 0.45 mmol, 88%. **^{1}H NMR (600 MHz, CD_2Cl_2)** δ = 8.02 (dd, *J* = 5.3, 1.9, 2H), 7.78 (d, *J* = 7.8 Hz, 2H), 7.74 (dt, *J* = 7.5 Hz, 2H), 7.35 – 7.29 (m, 4H), 7.25 (ddd, *J* = 8.2, 7.4, 1.6 Hz, 2H), 7.21 – 7.16 (m, 16H), 7.00 (td, *J* = 7.8, 0.9 Hz, 2H), 6.97 (ddd, *J* = 5.4, 4.1, 1.6 Hz, 2H), 6.93 (dtd, *J* = 8.2, 2.5, 1.1 Hz, 2H), 6.81 (dtd, *J* = 7.8, 4.0, 1.6 Hz, 2H) ppm. **^{13}C NMR (151 MHz, acetone-*d_6*)** δ = 157.9 (t, *J* = 6.1 Hz, 2C, Cq), 153.7 (m, 2C, Cq), 151.6 (t, *J* = 1.9 Hz, 2C, -CH), 139.4 (2C, -CH), 134.3 (2C, -CH), 133.8 (t, *J* = 8.1 Hz, 8C, -CH), 132.4 (2C, -CH), 131.0 (t, *J* = 16.7 Hz, 4C, -Cq), 130.6 (4C, -CH), 129.6 (2C, -CH), 129.2 (t, *J* = 4.8 Hz, 8C, -CH), 125.5 (t, *J* = 2.3 Hz, 2C, -CH), 124.8 (t, *J* = 13.8 Hz, 2C, C_q), 124.6 (2C, -CH), 120.7 (2C, -CH) ppm. **^{31}P NMR (243 MHz, CD_2Cl_2)** δ = -13.4 (*br* s, 1P), -144.5 (hept, *J* = 711 Hz, 1P) ppm. **^{19}F NMR (565 MHz, CD_2Cl_2)** δ = -73.5 (d, *J* = 710 Hz, 6F) ppm. **HRMS (ESI)** *m/z* Calcd for: $C_{46}H_{36}N_2O_2P_2SCu$ $[M - PF_6]^+$: 789.1323, found: 789.1320. **IR (neat)** v: 1740, 1579, 1435, 1218, 1096, 835 cm^{-1}. In good agreement with the literature with the analogous complex having BF_4 anion.[9]

Copper(I) [2-(2-diphenylphosphanylphenoxy)phenyl]-diphenylphosphane, 2,2'-dipyridylsulfone] hexafluorophosphate Complex 7. Following the general procedure from 0.49 mmol, Yield: 226 mg, 0.23 mmol, 48%. **^{1}H NMR: (600 MHz, acetone-*d*$_6$)** δ = 8.54 – 8.50 (*br* s, 2H), 8.42 (d, *J* = 7.9 Hz, 2H), 8.26 (t, *J* = 7.8 Hz, 2H), 7.60 – 7.55 (*br* s, 2H), 7.46 – 7.39 (m, 4H), 7.39 – 7.35 (m, 2H), 7.35 – 7.27 (m, 16H), 7.15 – 7.09 (*br* t, *J* = 7.5 Hz, 2H), 7.05 – 7.02 (m, 2H), 6.87 – 6.83 (m, 2H) ppm. **^{13}C NMR (125 MHz, acetone-*d*$_6$)** δ = 158.4 (t, *J* =6.0 Hz, 2C, Cq), 156.0 (2C, Cq), 152.9 (2C, -CH), 141.3 (2C, -CH), 134.9 (2C, -CH), 134.5 (t, *J* = 8.2 Hz, 8C, -CH), 133.3 (2C, -CH), 131.3 (4C, -CH), 131 (t, *J* = 17.1 Hz, 4C, Cq), 130.0 – 129.9 (*br* s, 2C, -CH), 129.8 (t, *J* = 4.9 Hz, 8C, _CH), 126.2 (t, *J* = 2.3 Hz, 2C, -CH), 125.7 (2C, -CH), 124.8 (t, *J* = 15.4 Hz, 2C, Cq), 121.1 (2C, -CH) ppm. **^{31}P NMR (243 MHz, acetone-*d*$_6$)** δ = -14.9 (s, 2P), -144.3 (hept, *J* = 708 Hz, 1P) ppm. **^{19}F NMR (565 MHz, acetone-d$_6$)** δ = -72.6 (d, *J* = 709 Hz, 6F) ppm. **IR (neat)** ν = 1739, 1714, 1588, 1434, 1365, 1316, 1206, 836, 747 cm^{-1}. In good agreement with the literature with the analogous complex having BF_4 anion.[9]

NMR spectra of ligands **L1**, **L3**-**L7**

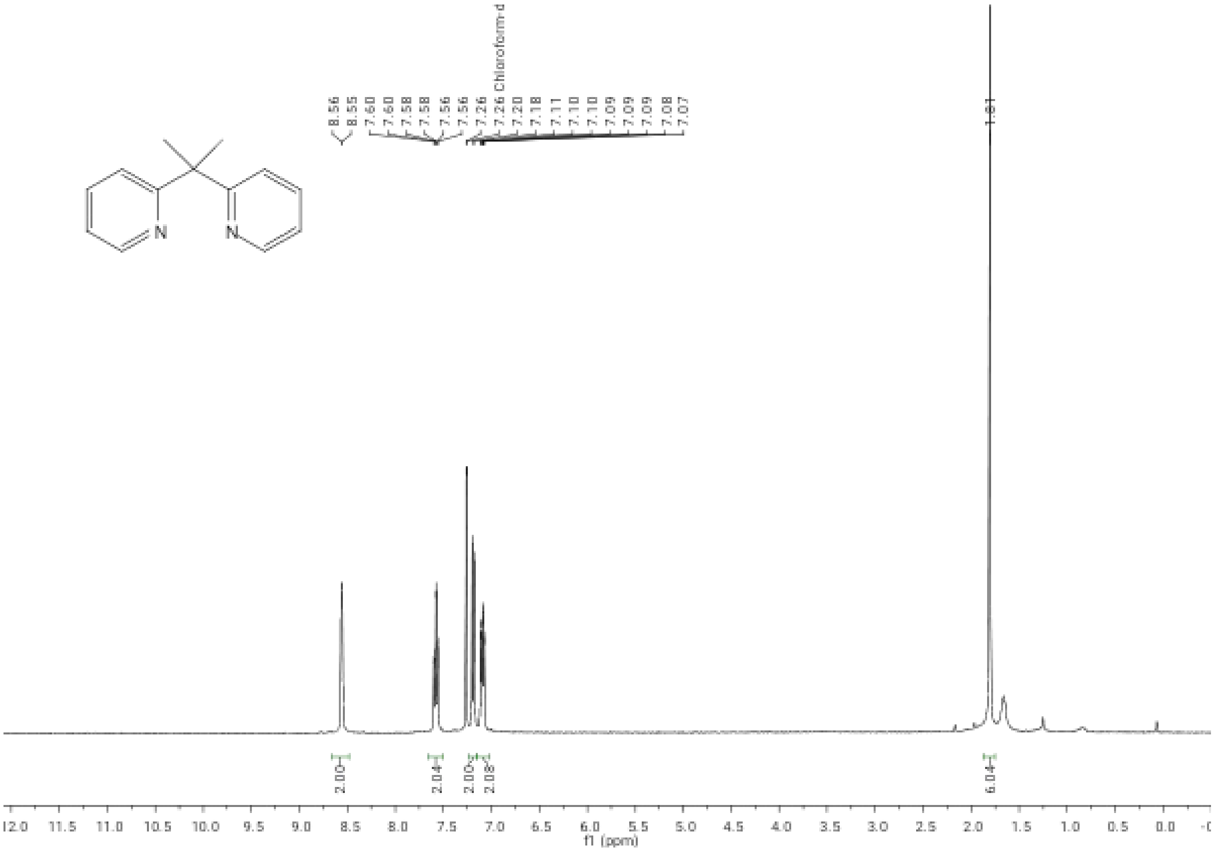

Figure S1: ^{1}H NMR (400MHz, $CDCl_3$) spectrum of 2,2'-(propane-2,2-diyl) dipyridine **L1**.

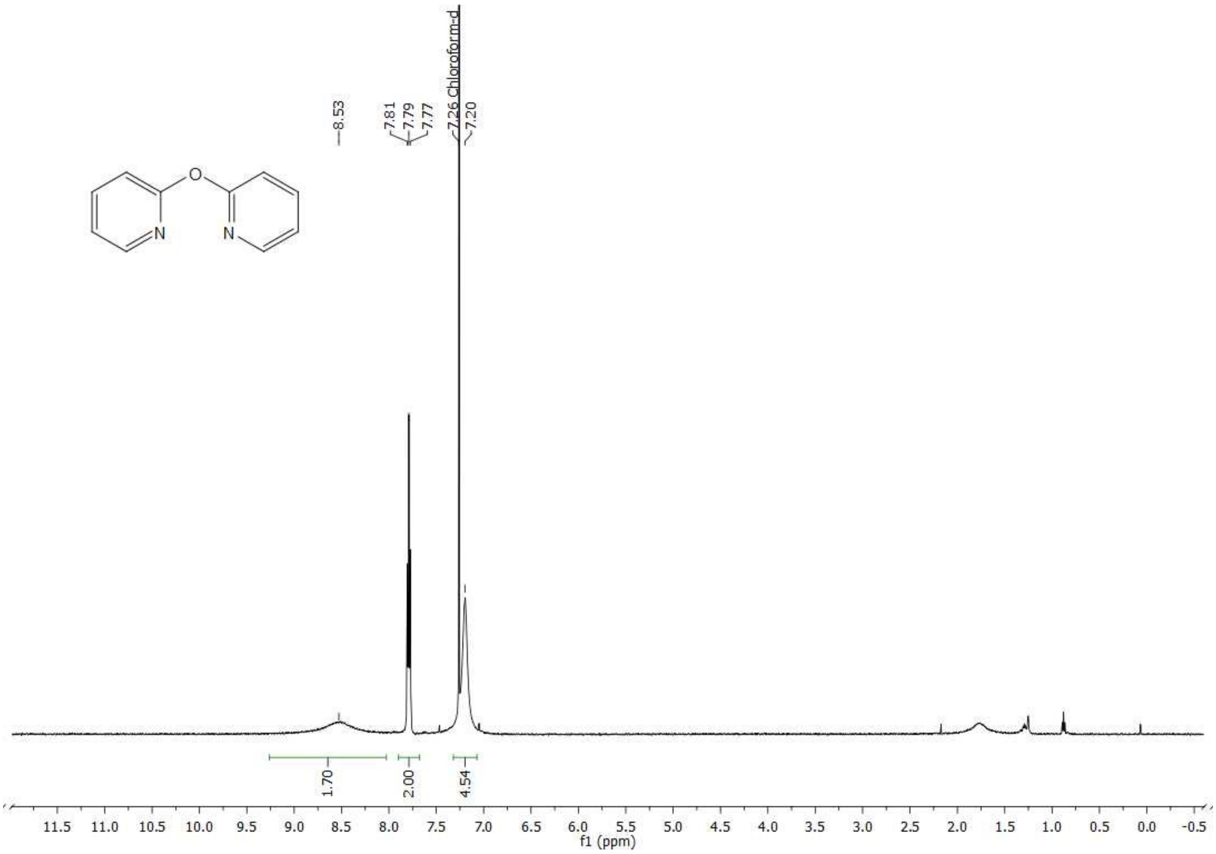

Figure S2: ^{1}H NMR (500 MHz, $CDCl_3$) spectrum of 2,2'-oxydipyridine **L3**.

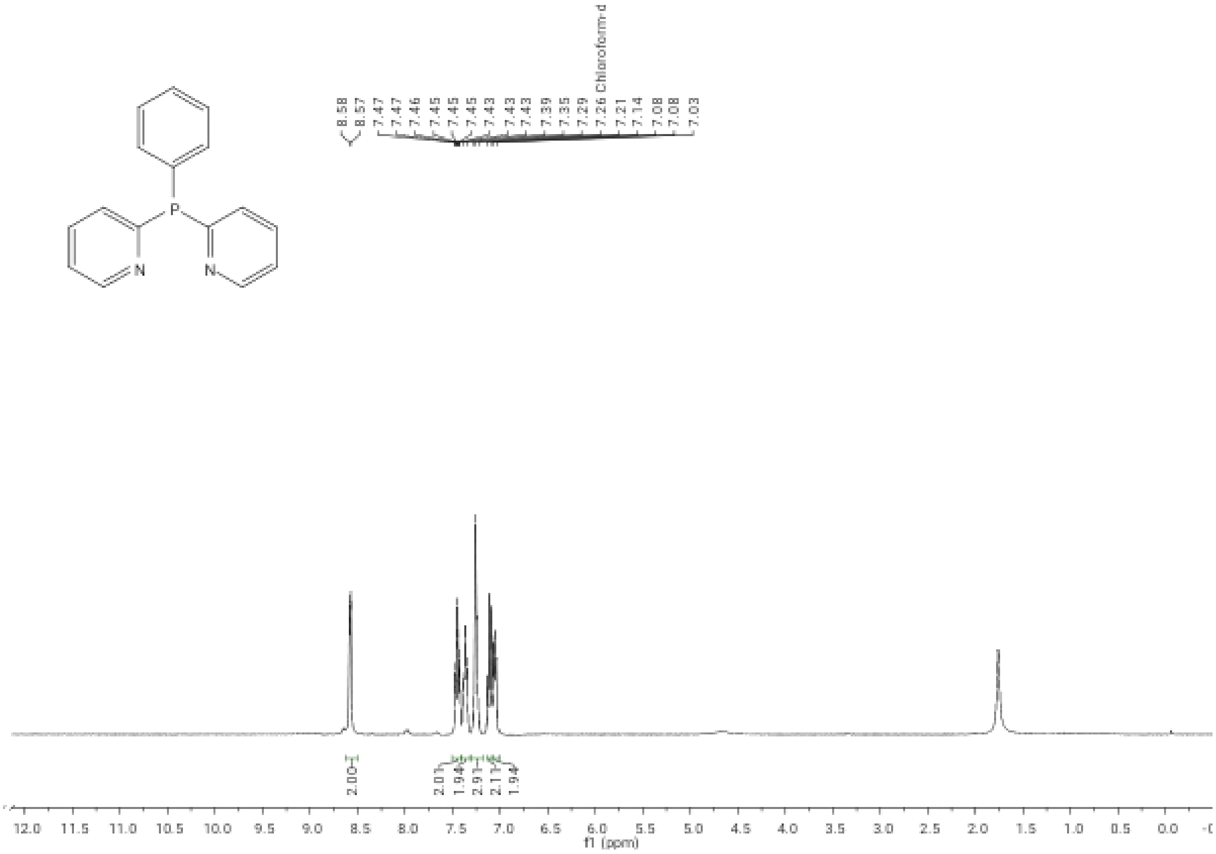

Figure S3: ^{1}H NMR (400 MHz, $CDCl_3$) spectrum of 2,2’-(phenylphosphanediyl)dipyridine **L4**.

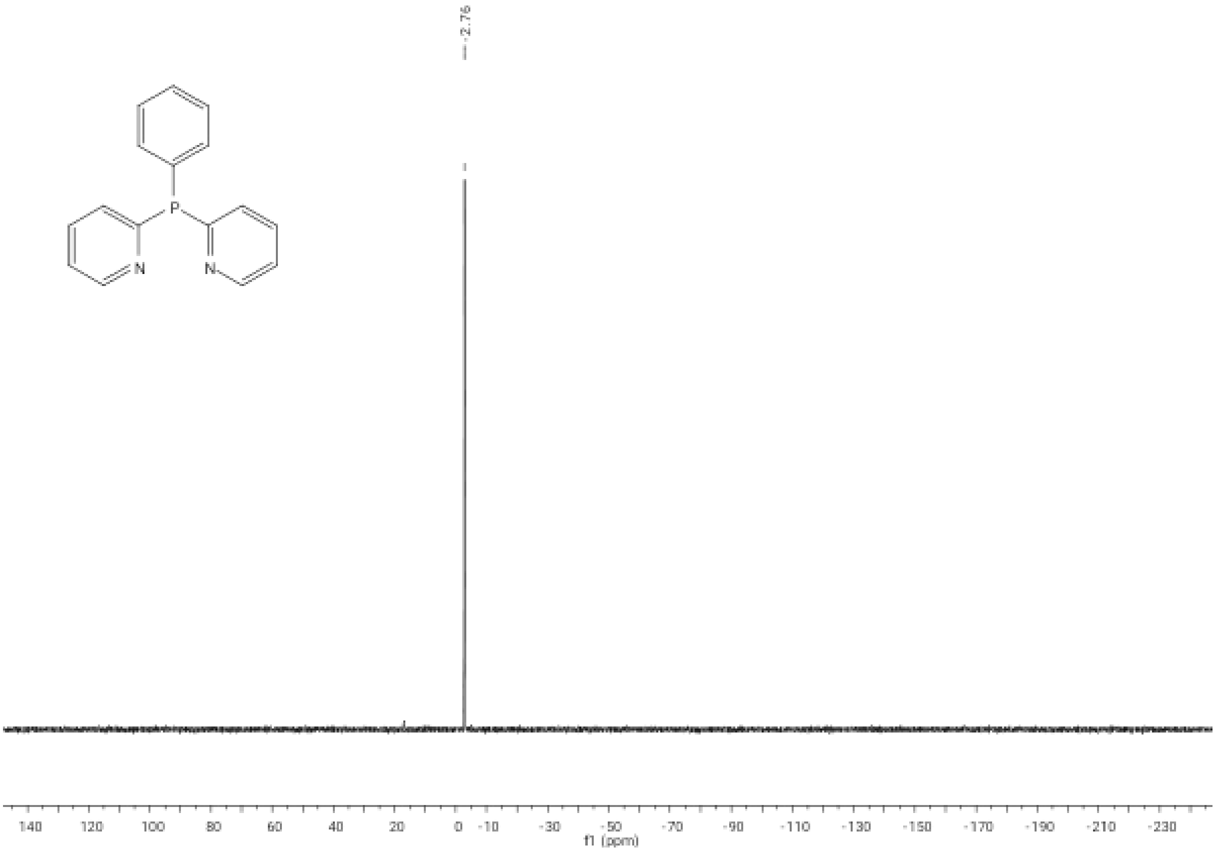

Figure S4: ^{31}P NMR spectrum of 2,2’-(phenylphosphanediyl)dipyridine **L4**.

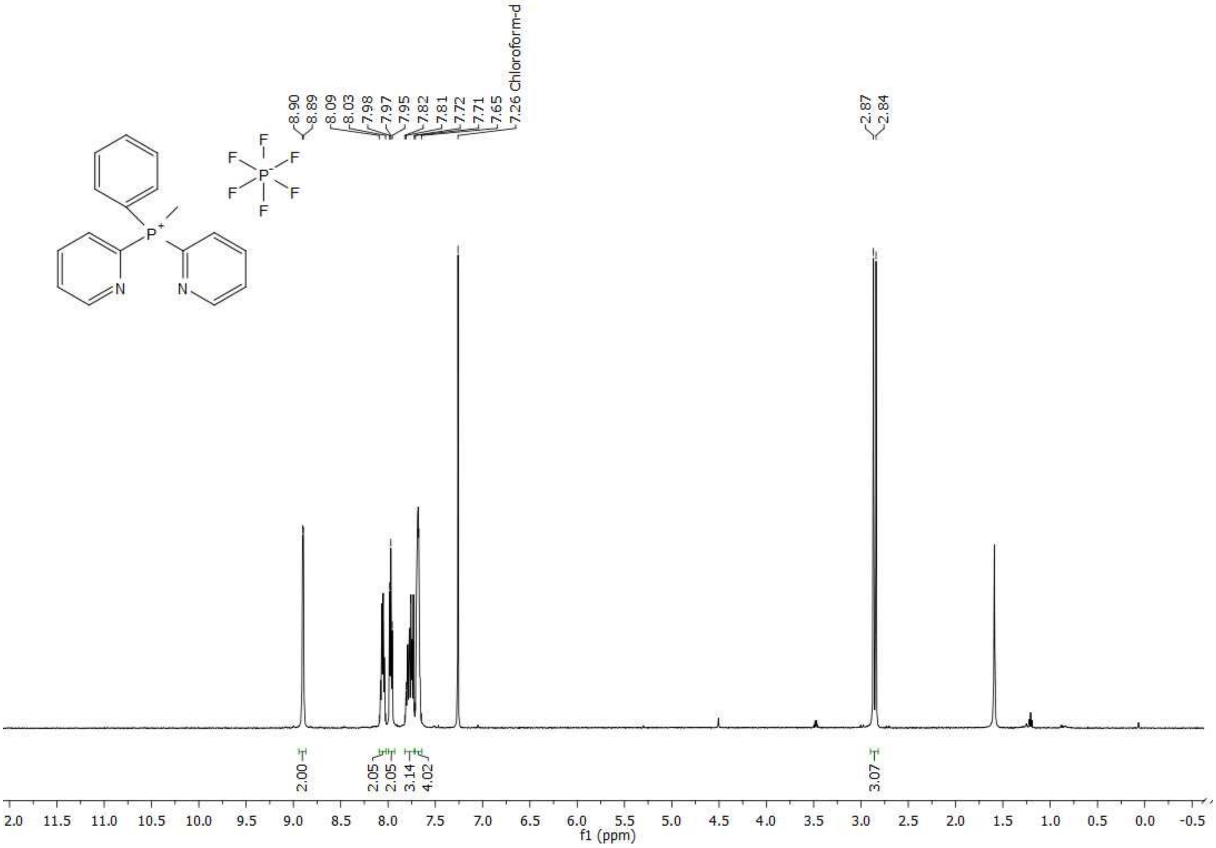

Figure S5: ^1H NMR (500 MHz, $CDCl_3$) spectrum of methyl(phenyl)di(pyridin-2-yl)phosphonium hexafluorophosphate **L5**.

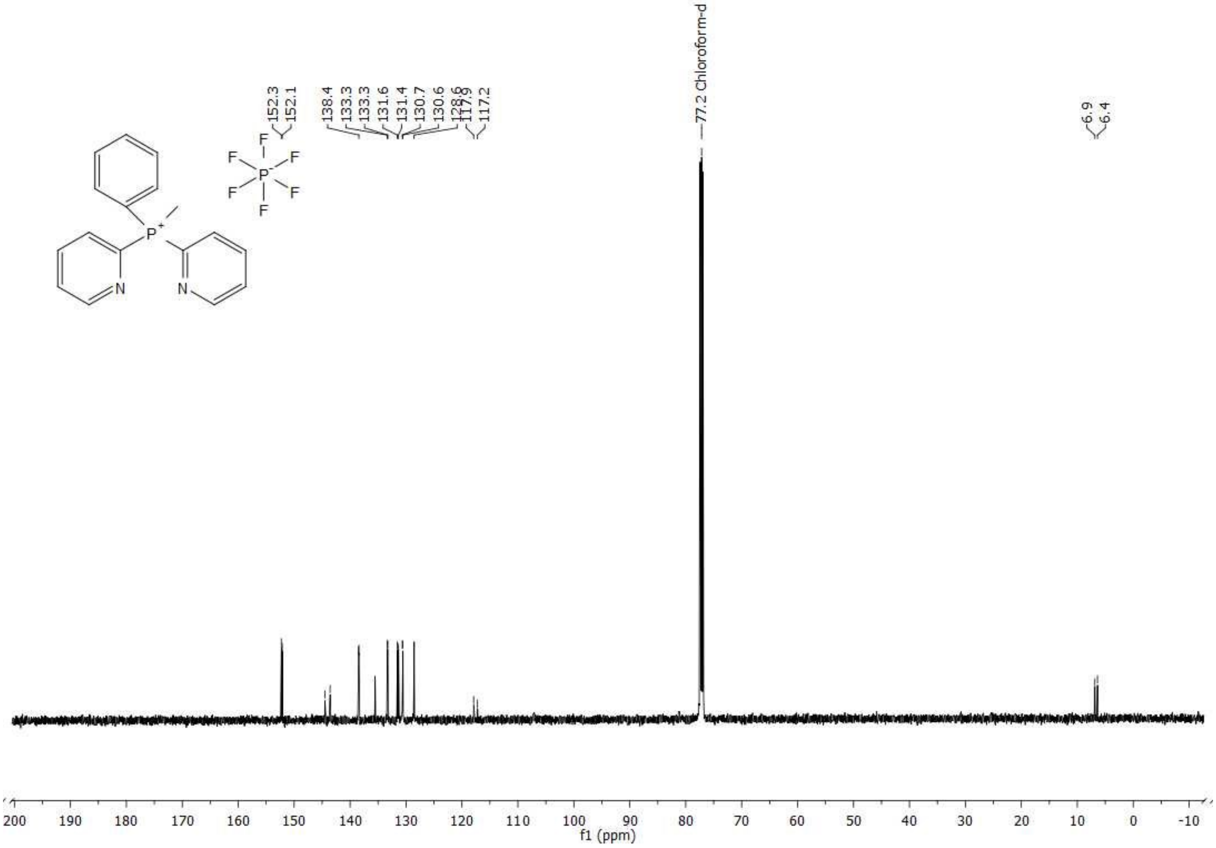

Figure S6: ^{13}C NMR (126 MHz, $CDCl_3$) spectrum of methyl(phenyl)di(pyridin-2-yl)phosphonium hexafluorophosphate **L5**.

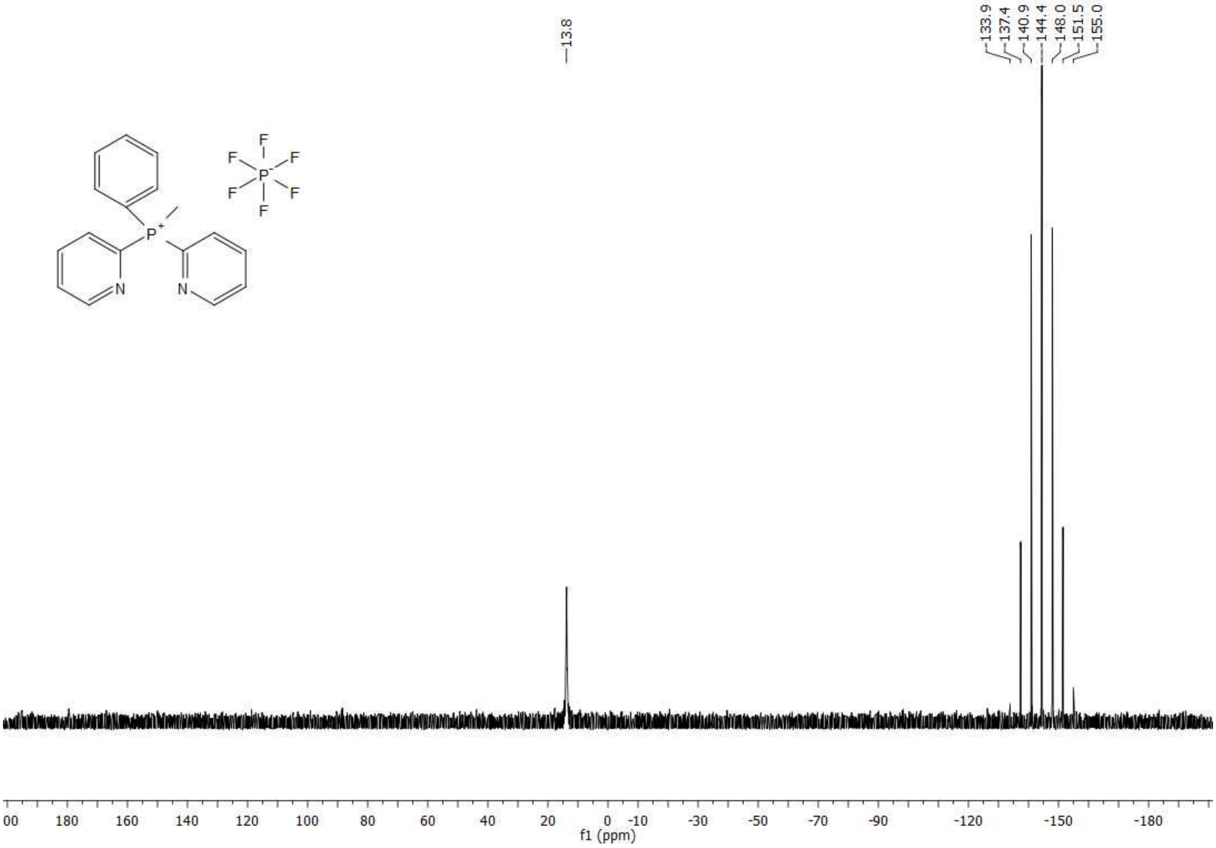

Figure S7: ^{31}P NMR (202 MHz, $CDCl_3$) spectrum of methyl(phenyl)di(pyridin-2-yl)phosphonium hexafluorophosphate **L5**.

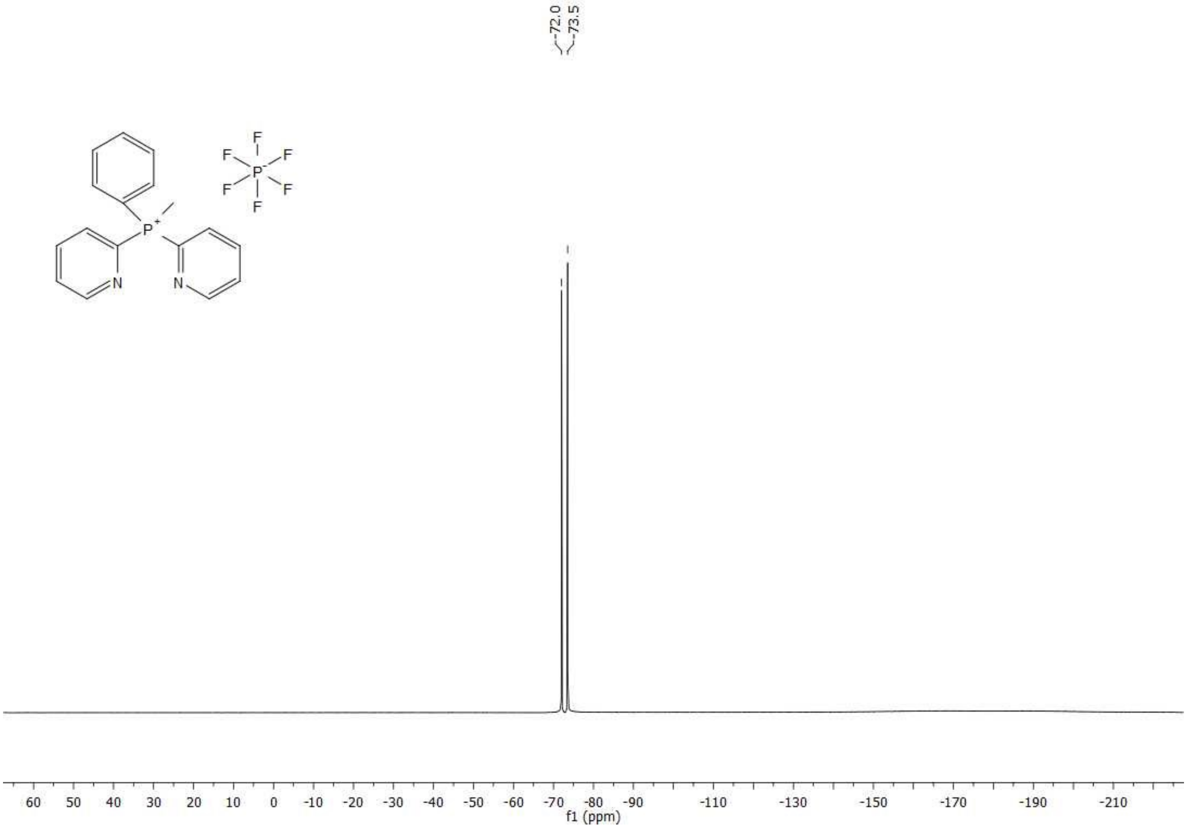

Figure S8: ^{19}F NMR (471 MHz, $CDCl_3$) spectrum of methyl(phenyl)di(pyridin-2-yl)phosphonium hexafluorophosphate **L5**.

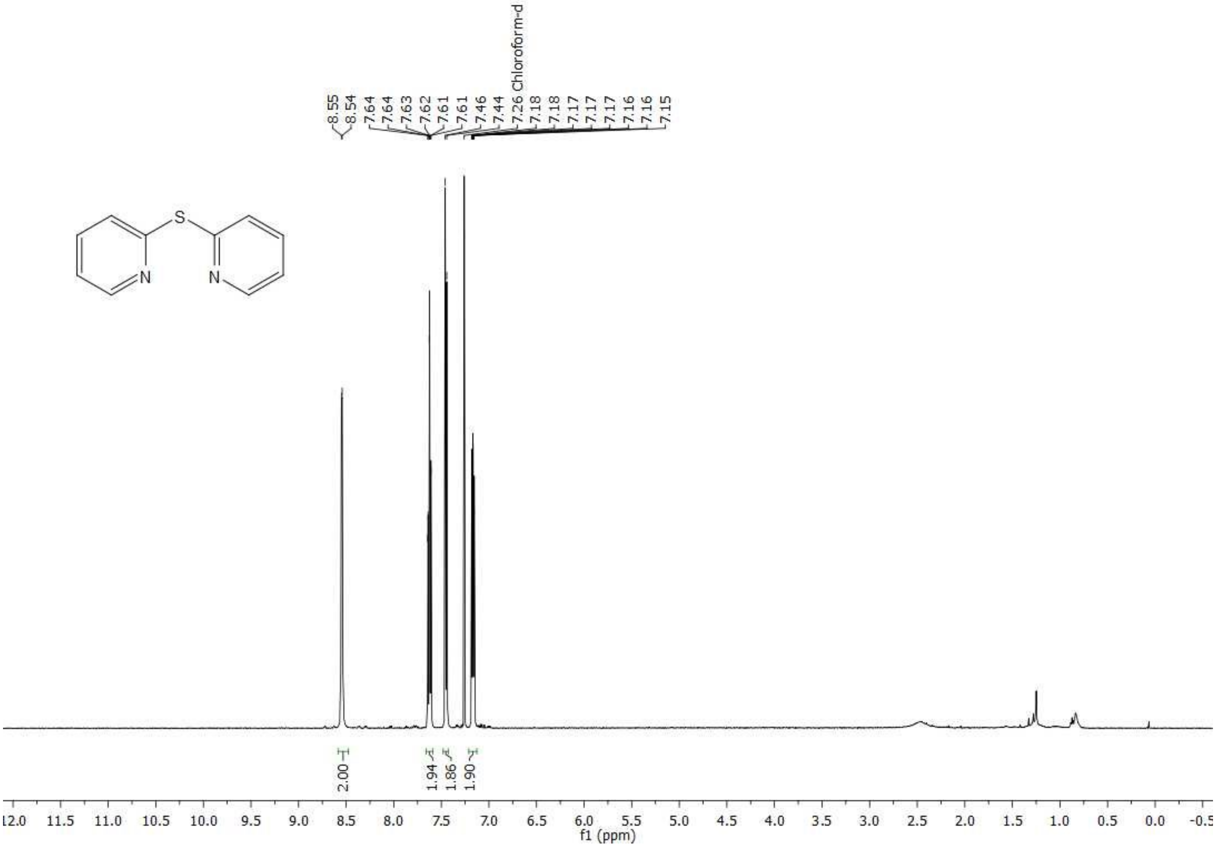

Figure S9: ^{1}H NMR (500 MHz, $CDCl_3$) spectrum of di(pyridin-2-yl)sulfane **L6**.

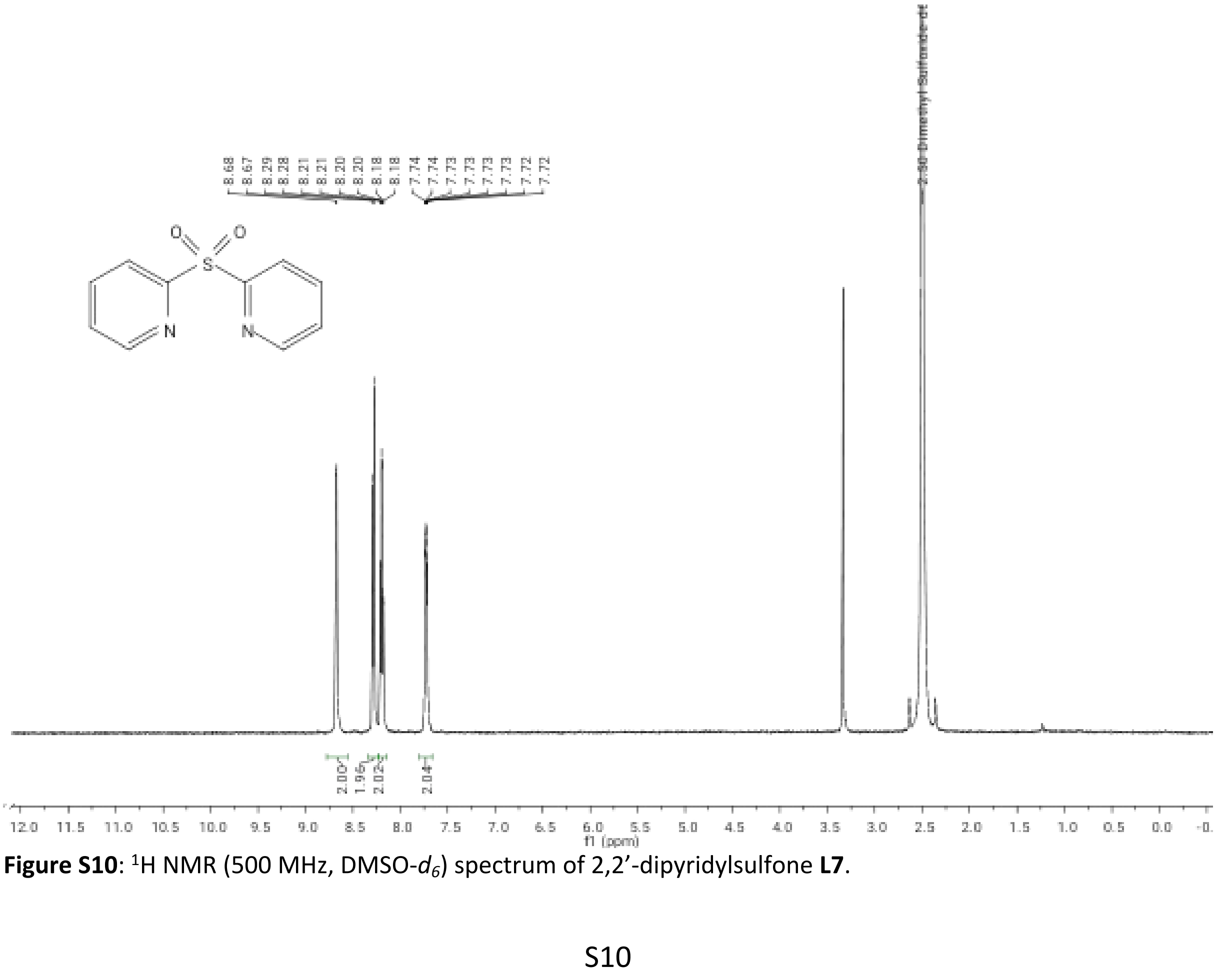

Figure S10: ^{1}H NMR (500 MHz, DMSO-d_6) spectrum of 2,2’-dipyridylsulfone **L7**.

NMR spectra of complexes **1-7**

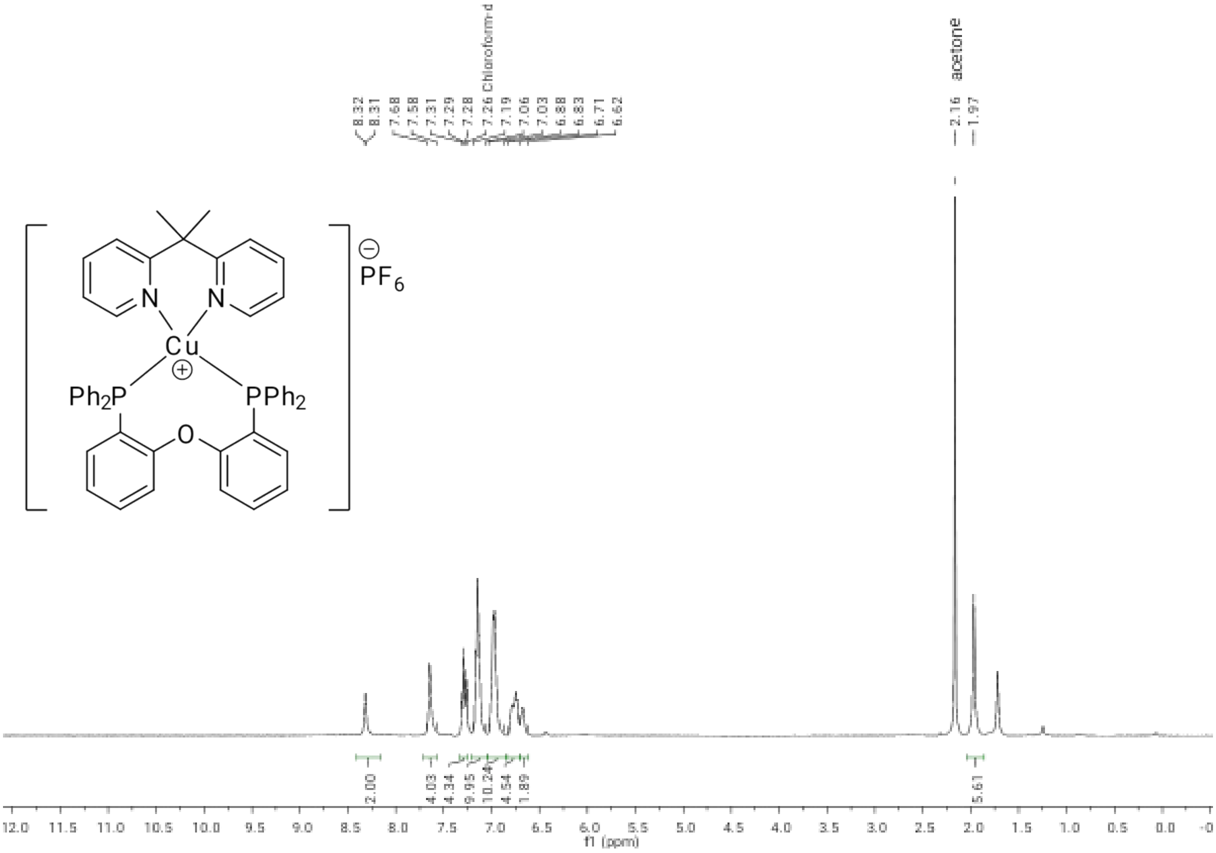

Figure **S11**: ^{1}H NMR (400 MHz, $CDCl_3$) spectrum of complex **1**.

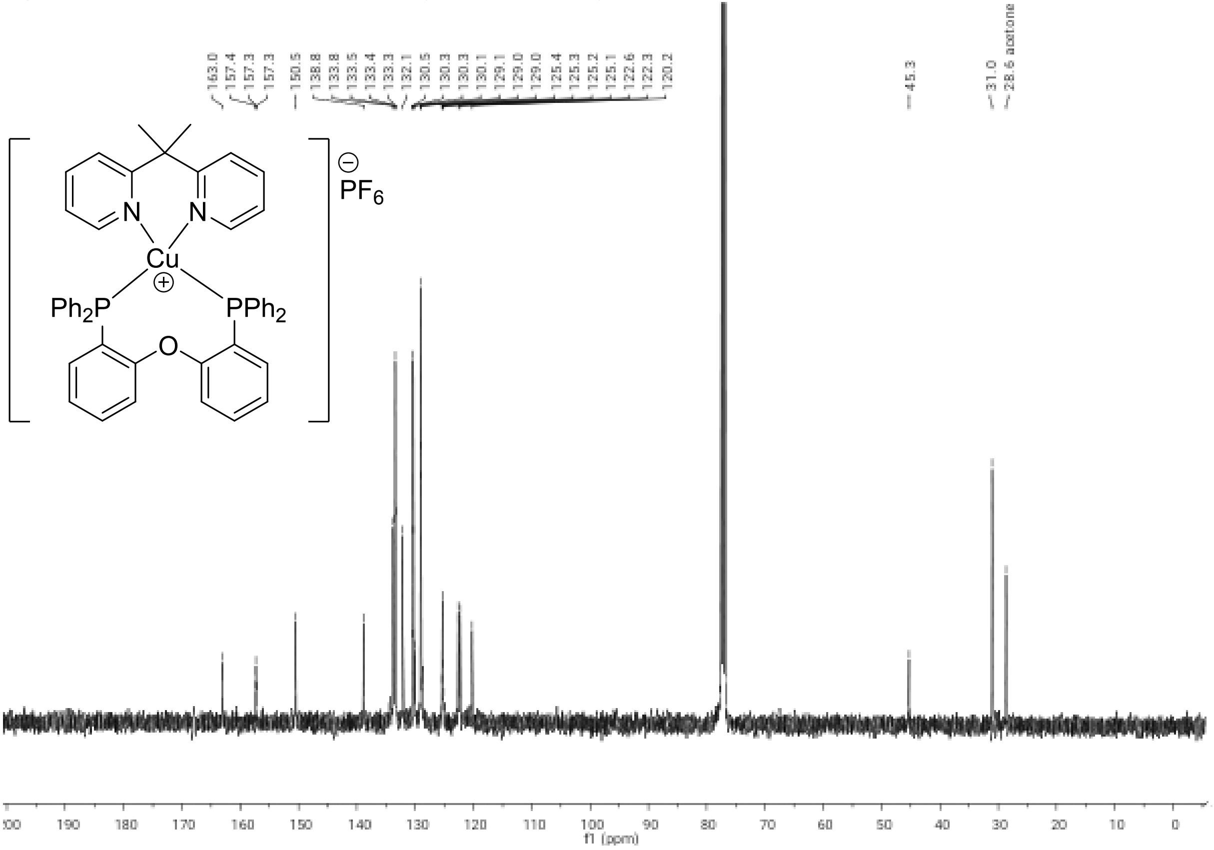

Figure **S12**: ^{13}C NMR (101 MHz, $CDCl_3$) spectrum of complex **1**.

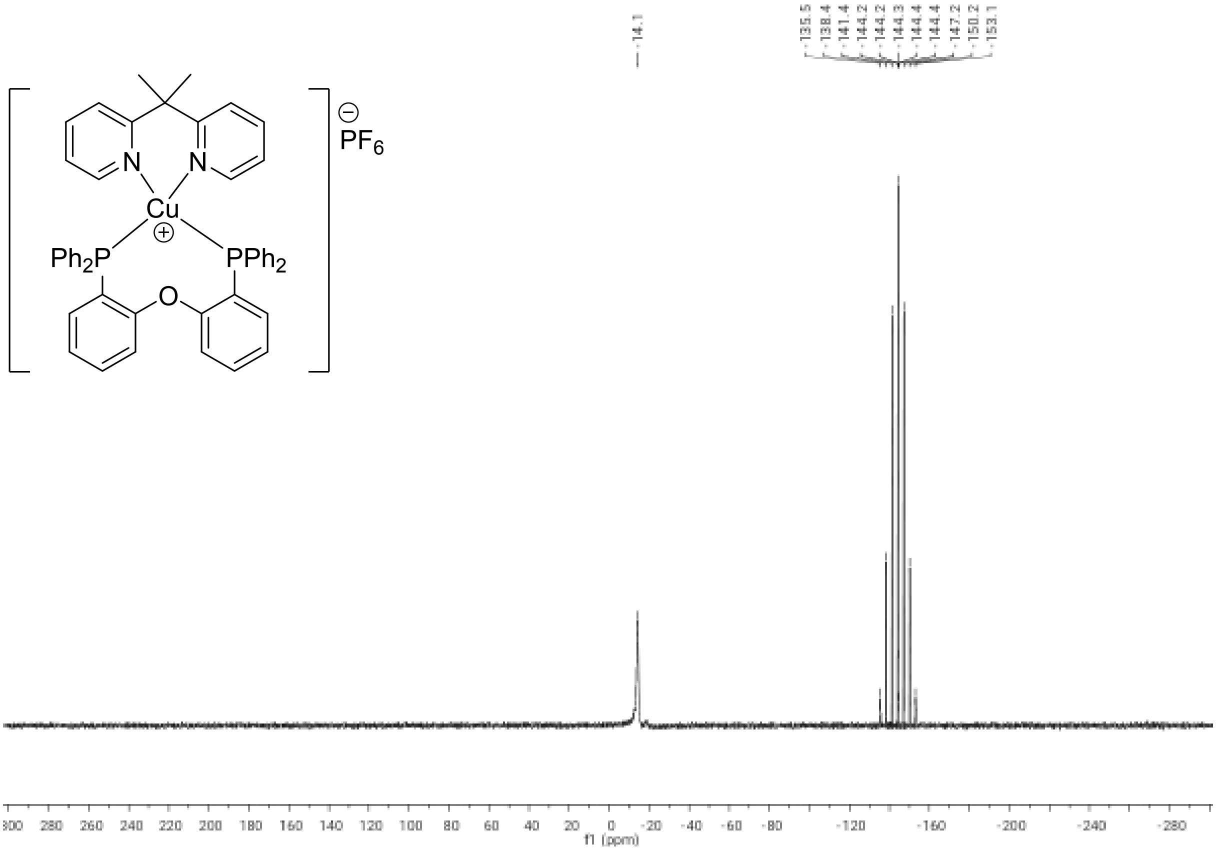

Figure S13: ^{31}P NMR (243 MHz, $CDCl_3$) spectrum of complex **1**.

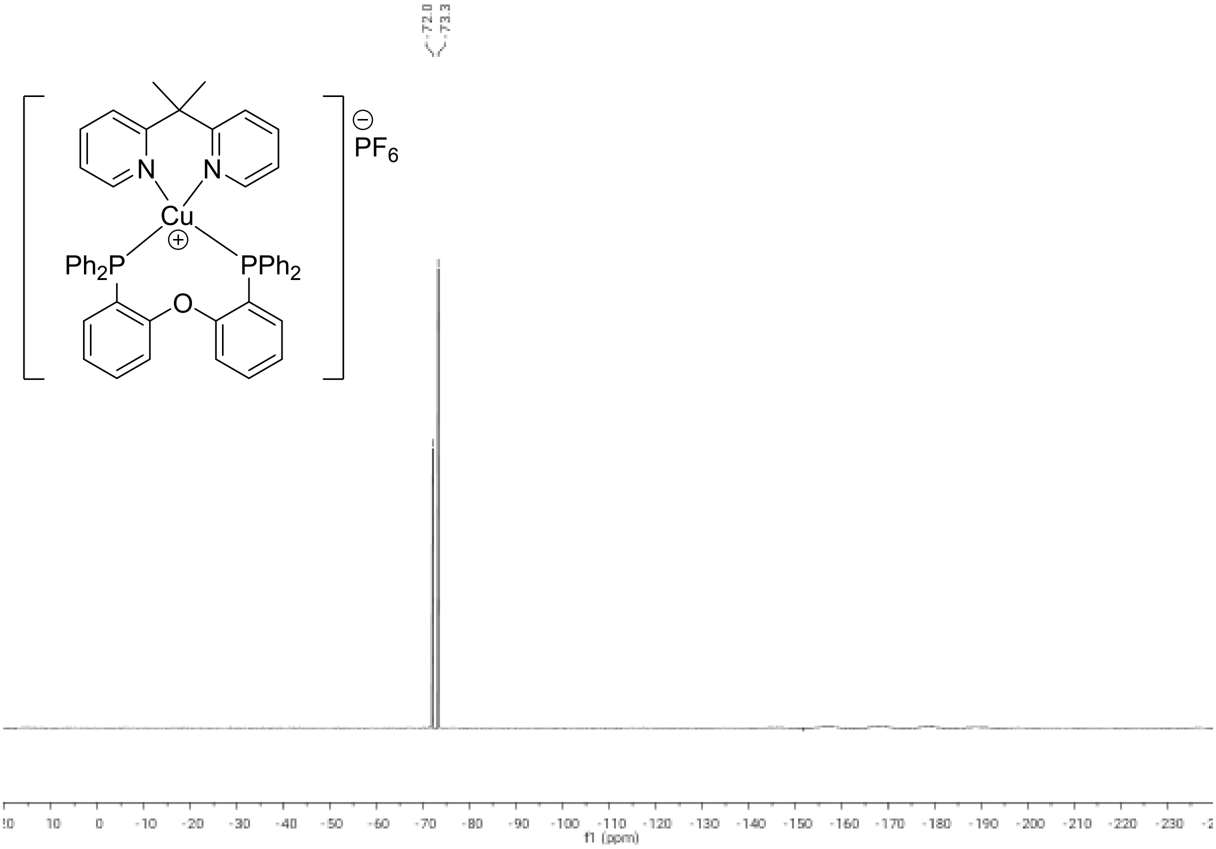

Figure S14: ^{19}F NMR spectrum (565 MHz, acetone-d_6) of complex **1**.

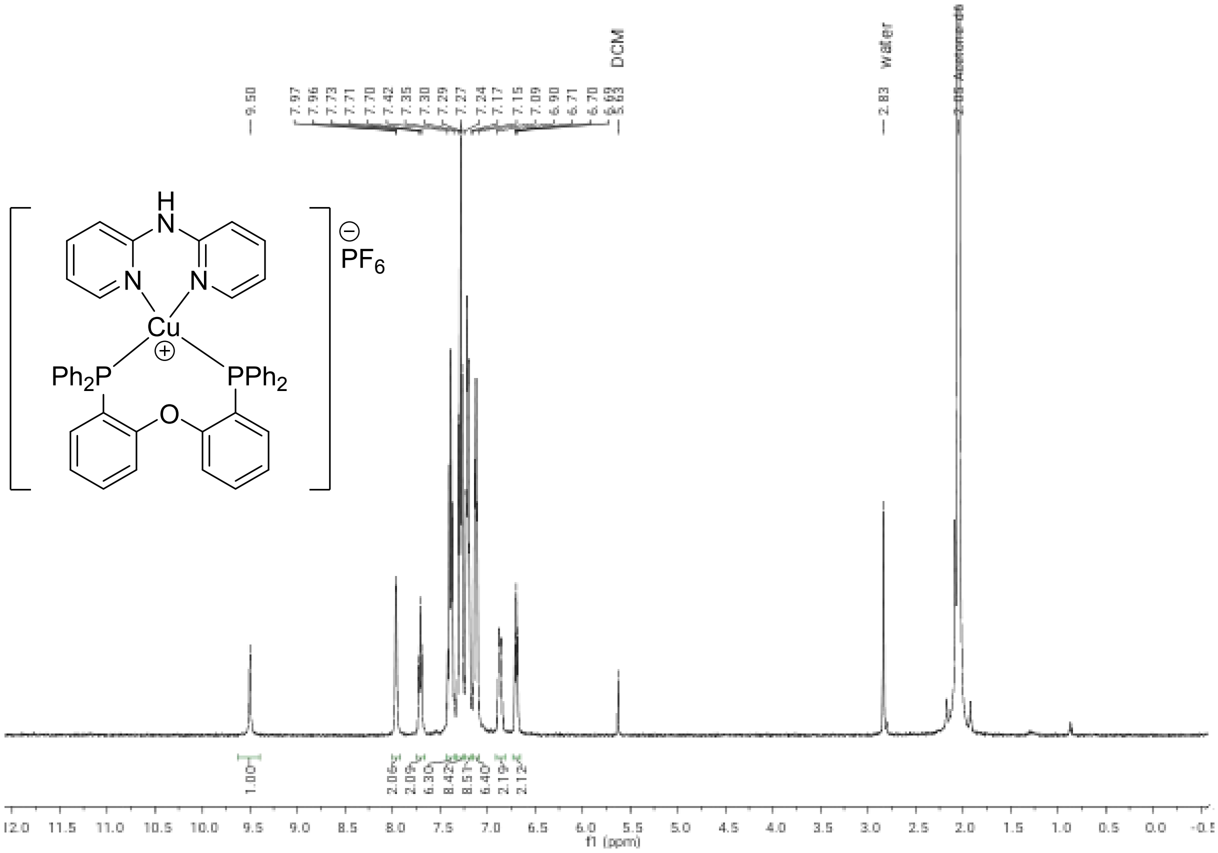

Figure S15: ^{1}H NMR (500 MHz, acetone-d_6) spectrum of complex **2**.

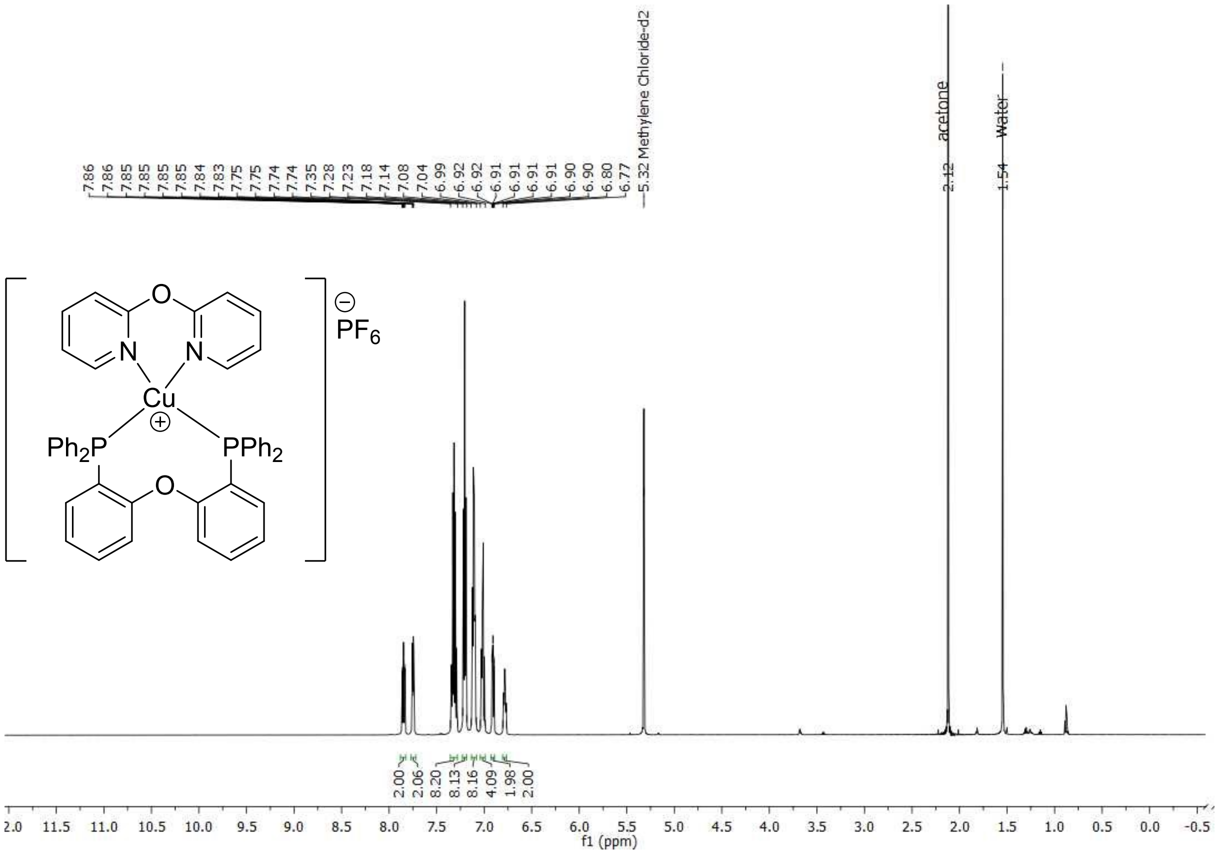

Figure S16: ^{1}H NMR (600 MHz, CD_2Cl_2) spectrum of complex **3**.

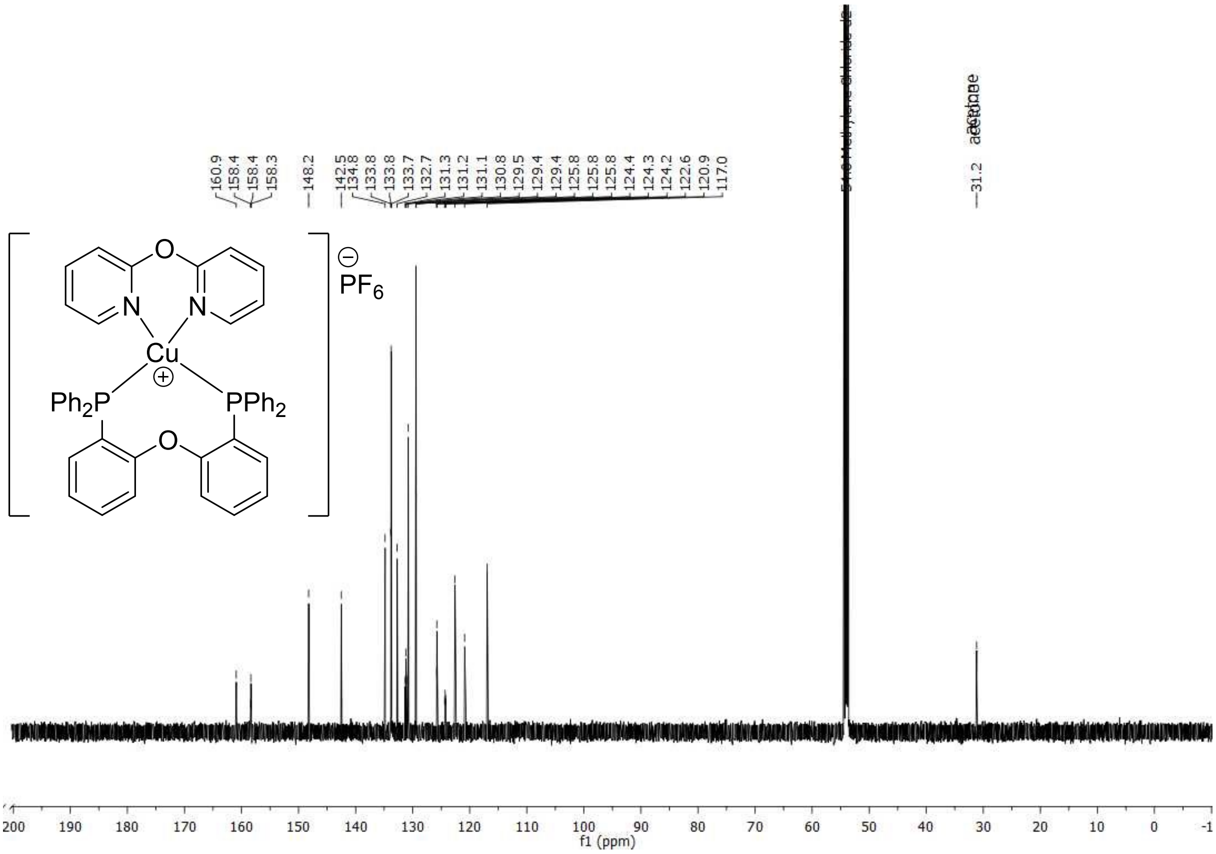

Figure S17: ^{13}C NMR (151 MHz, CD_2Cl_2) spectrum of complex **3**.

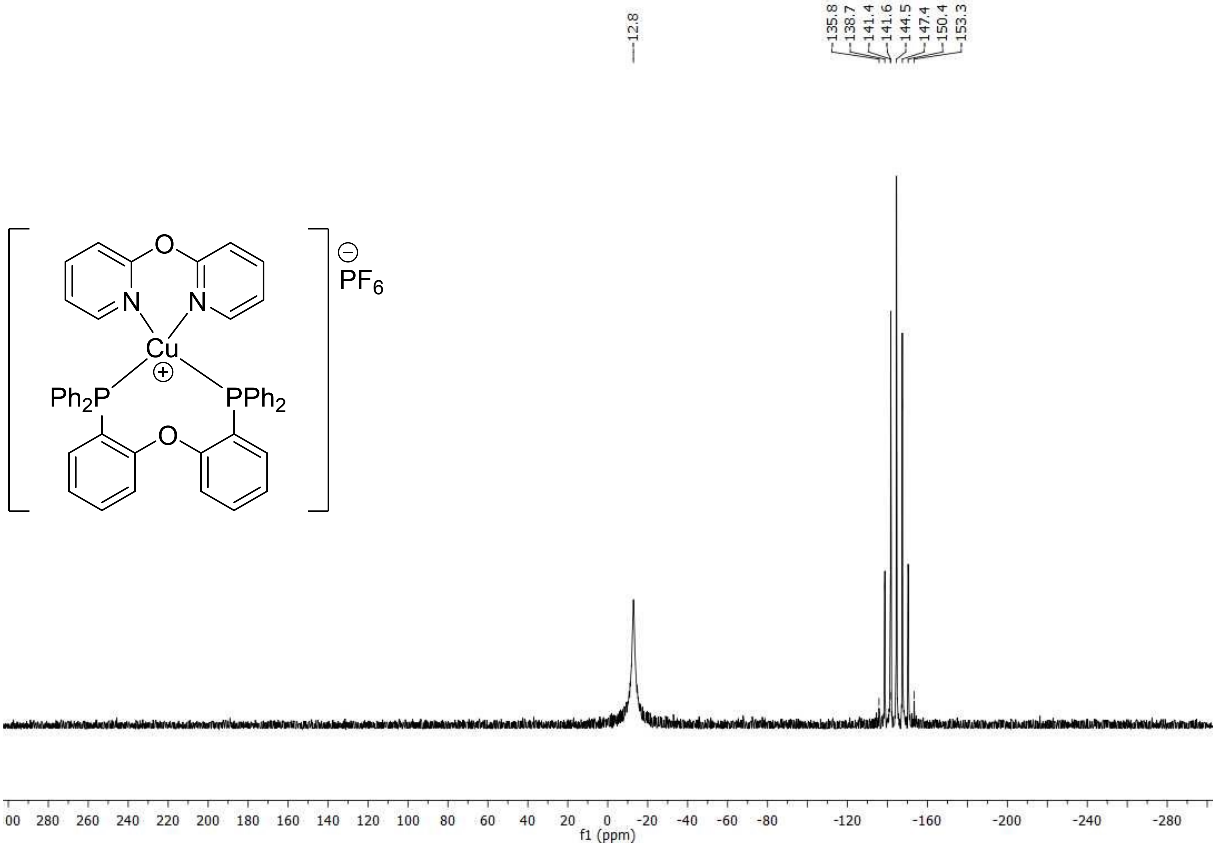

Figure S18: ^{31}P NMR (243 MHz, CD_2Cl_2) spectrum of complex **3**.

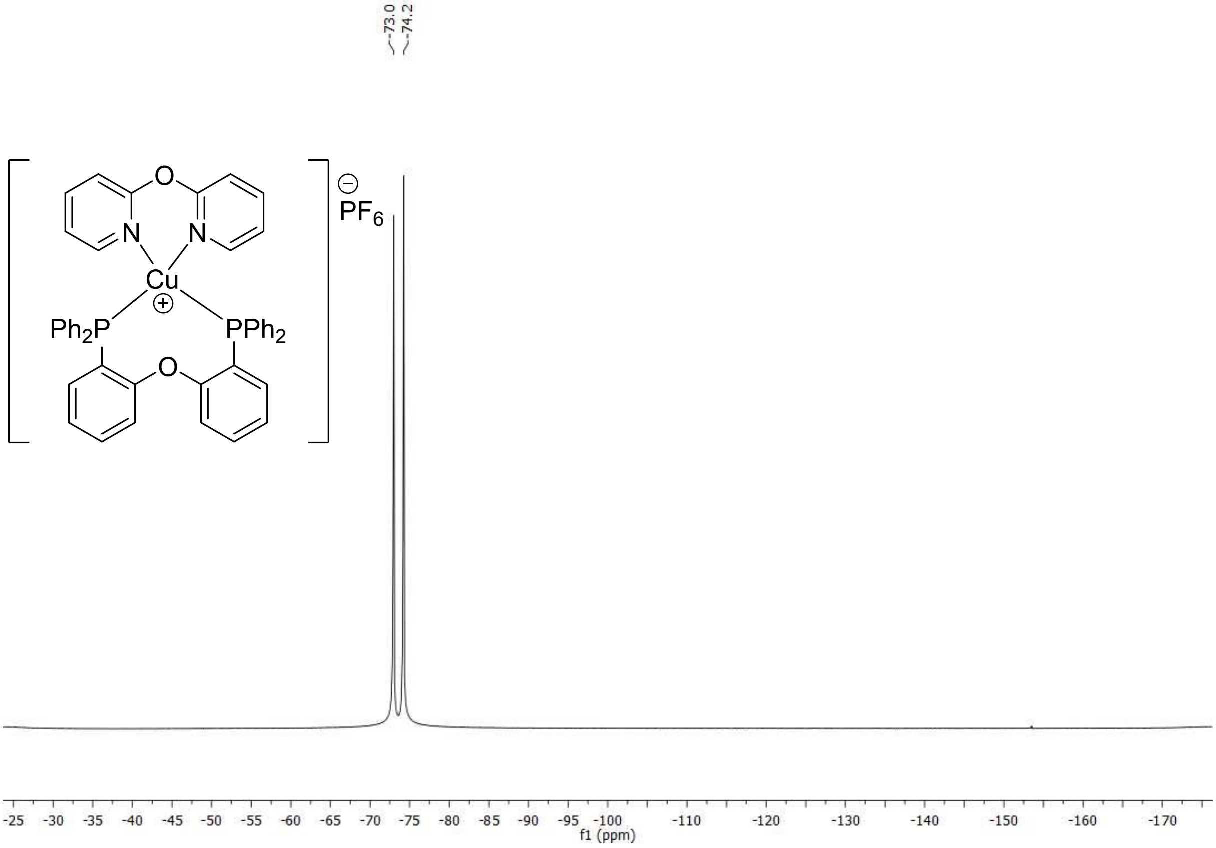

Figure S19: ^{19}F NMR (565 MHz, CD_2Cl_2) spectrum of complex **3**.

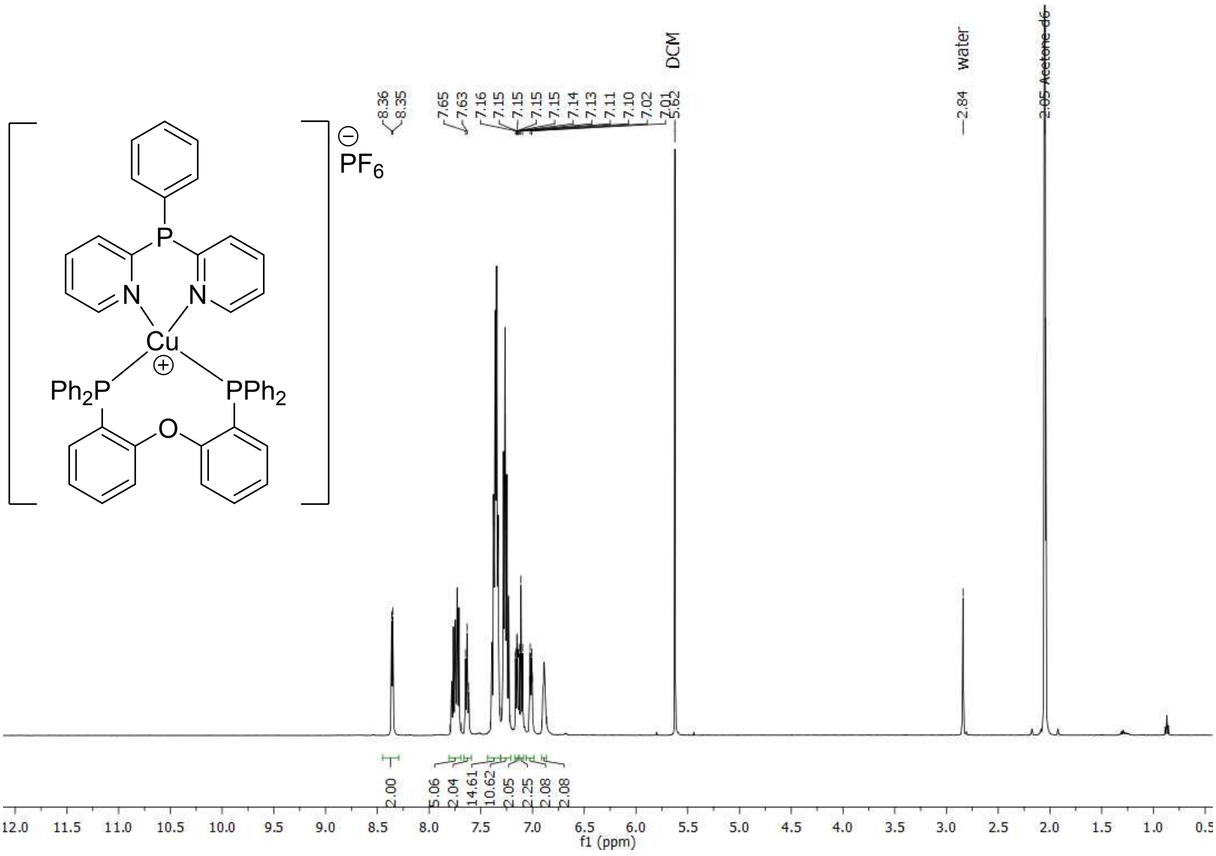

Figure S20: ^{1}H NMR (500 MHz, acetone-d_6) spectrum of complex **4**.

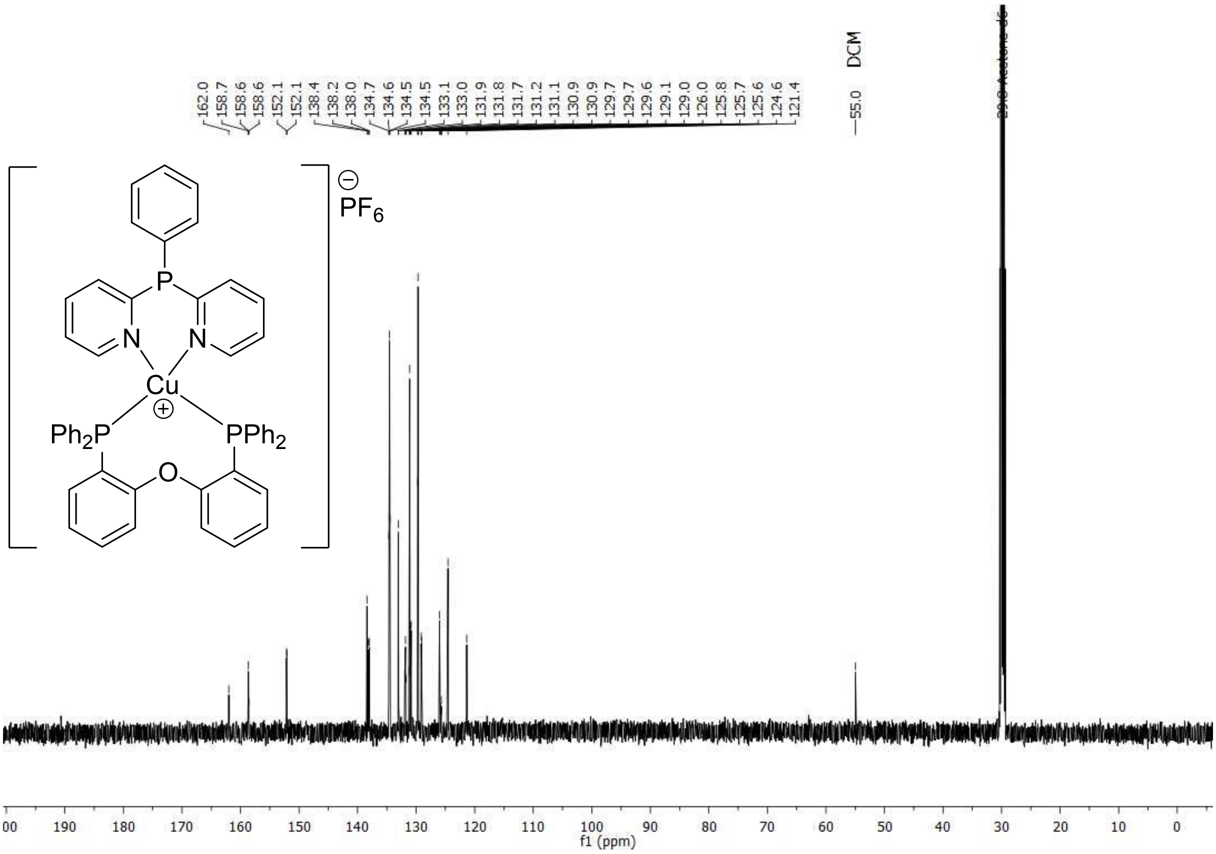

Figure S21: ^{13}C NMR (126 MHz, acetone-d_6) spectrum of complex **4**.

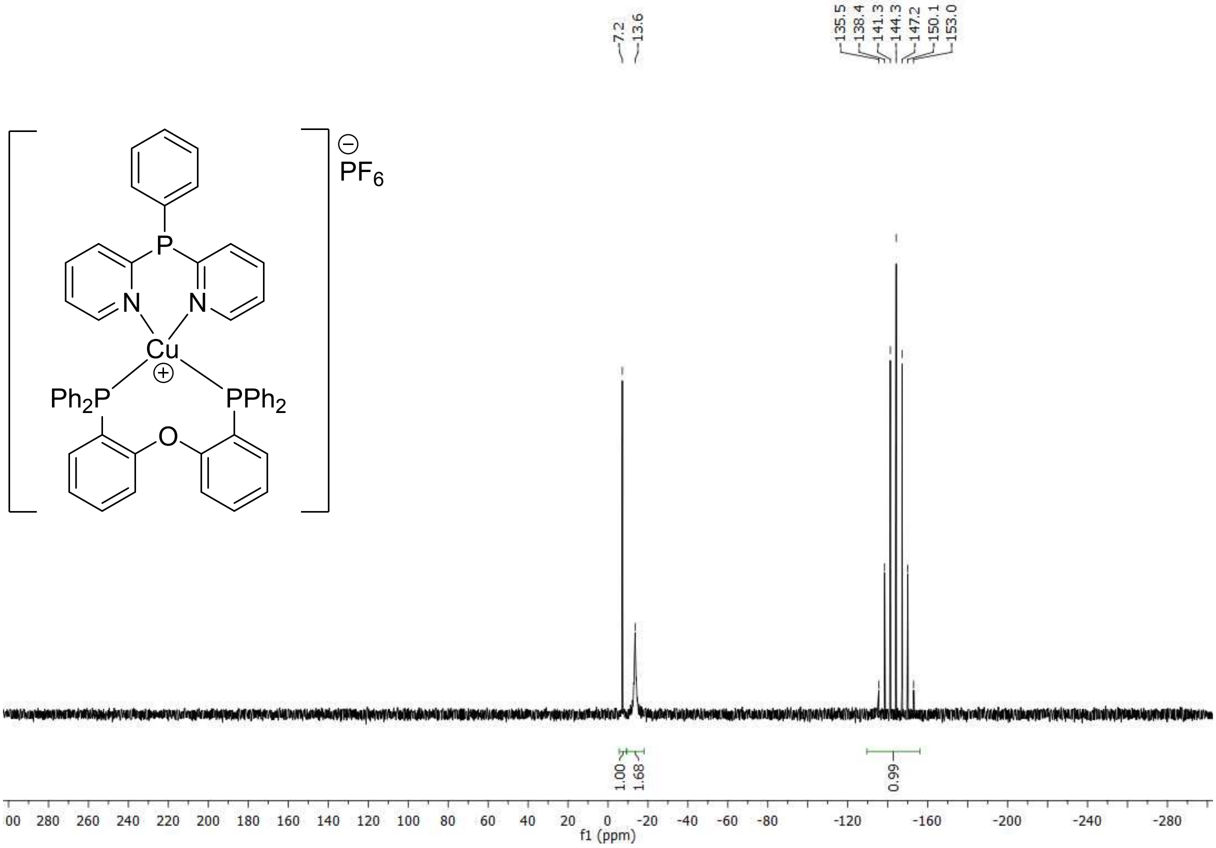

Figure S22: ^{31}P NMR (243 MHz, acetone-d_6) spectrum of complex **4**.

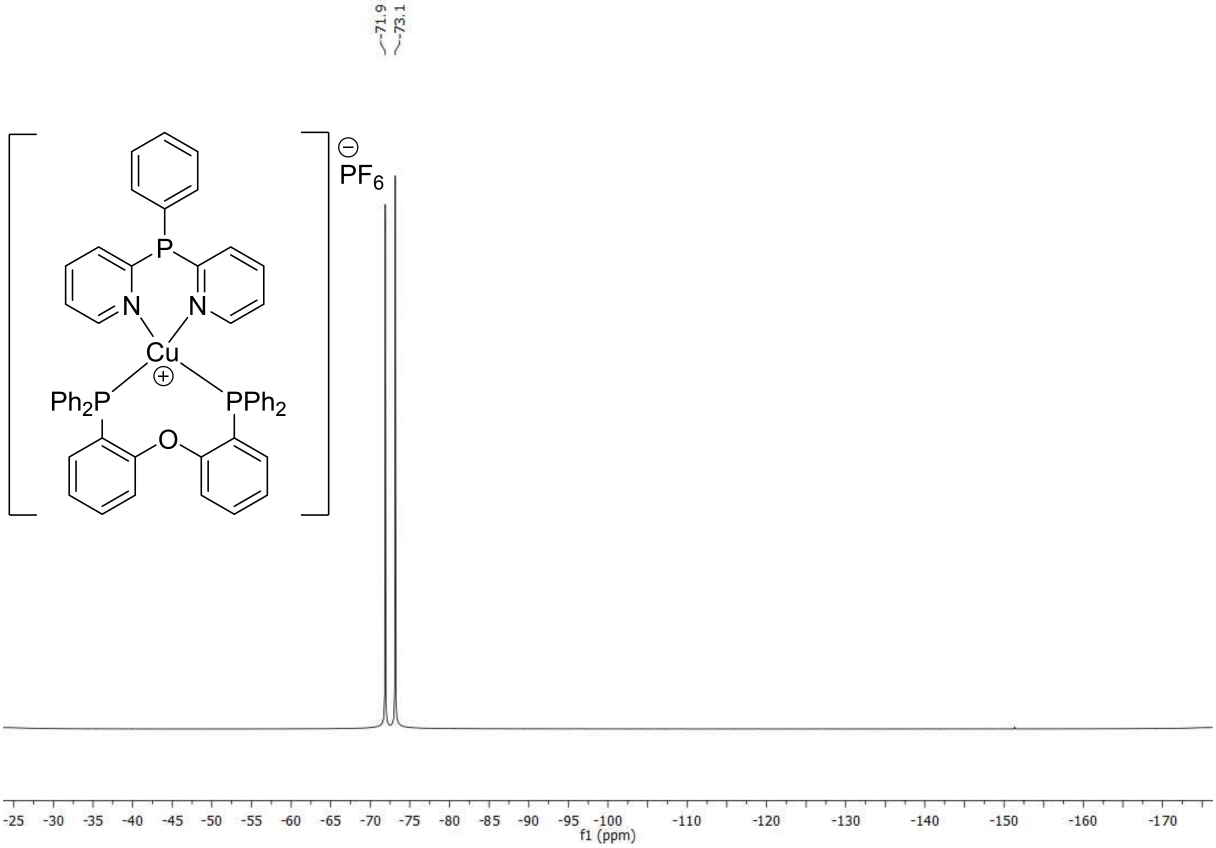

Figure S23: ^{19}F NMR (565 MHz, CD_2Cl_2) spectrum of complex **4**.

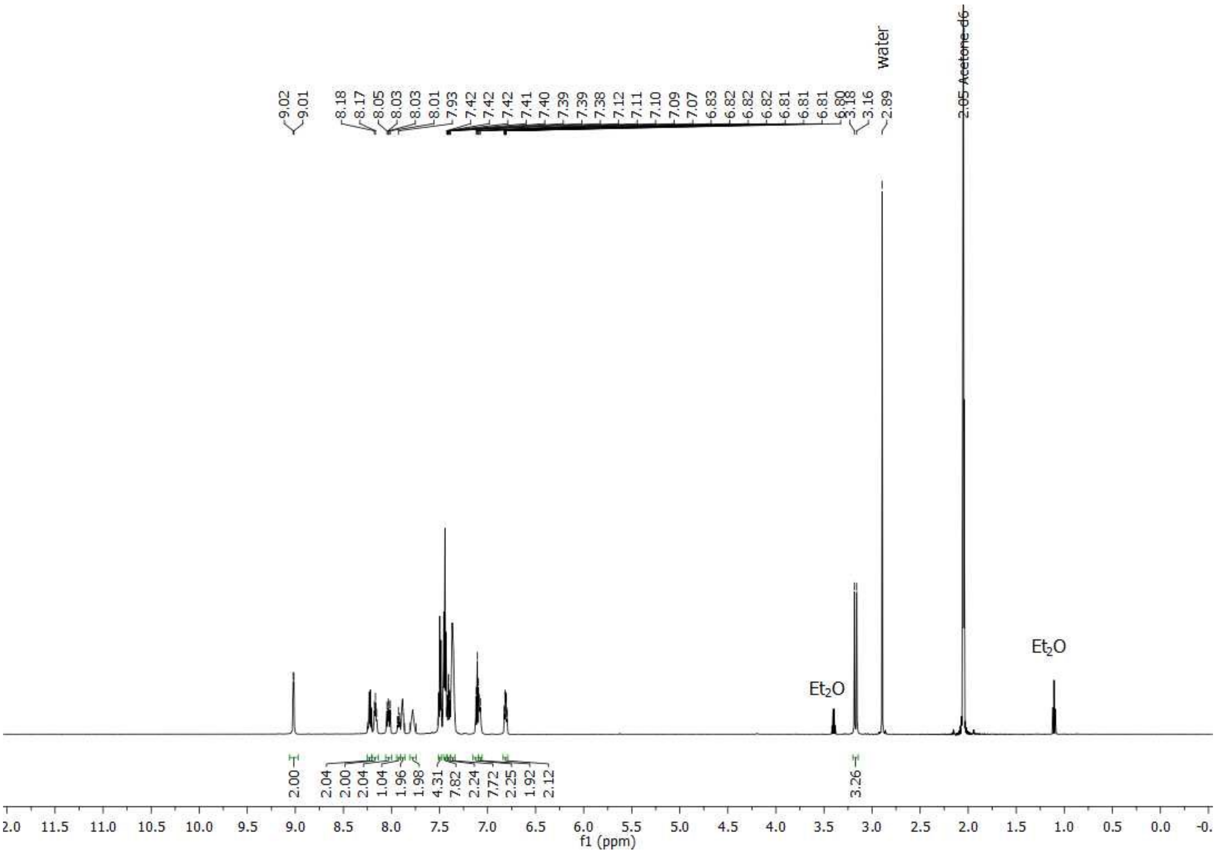

Figure S24: ^{1}H NMR (600 MHz, acetone-d_6) spectrum of complex **5**.

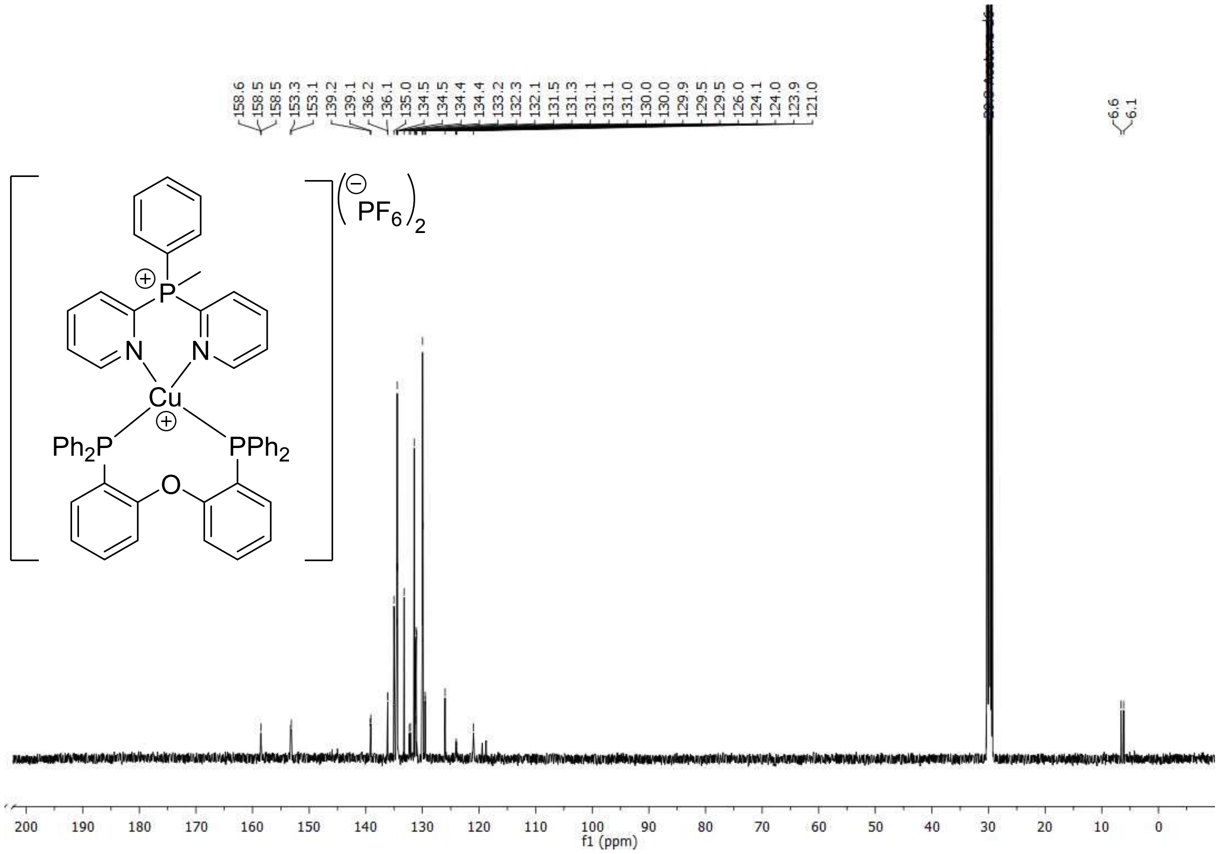

Figure S25: ^{13}C NMR (125 MHz, acetone-*d₆*) spectrum of complex **5**.

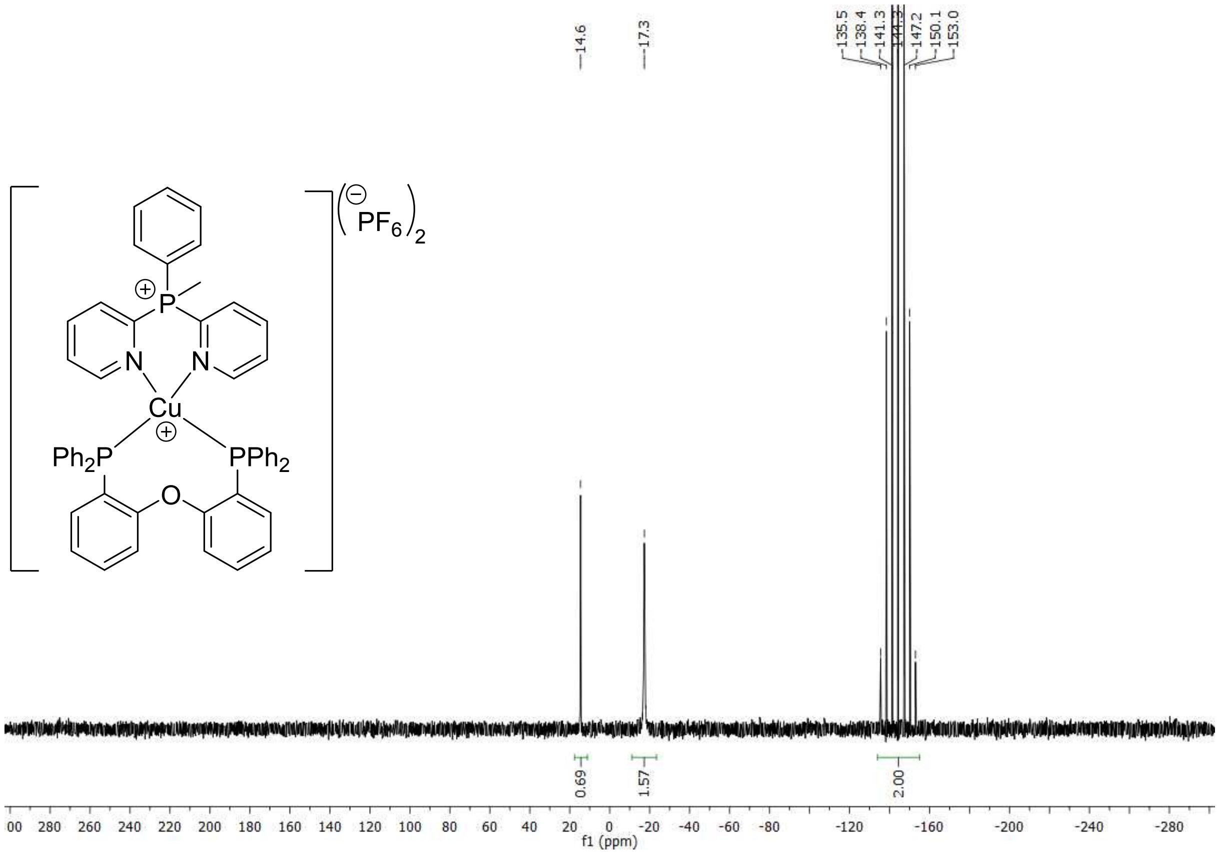

Figure S26: ^{31}P NMR (243 MHz, acetone-*d₆*) spectrum of complex **5**.

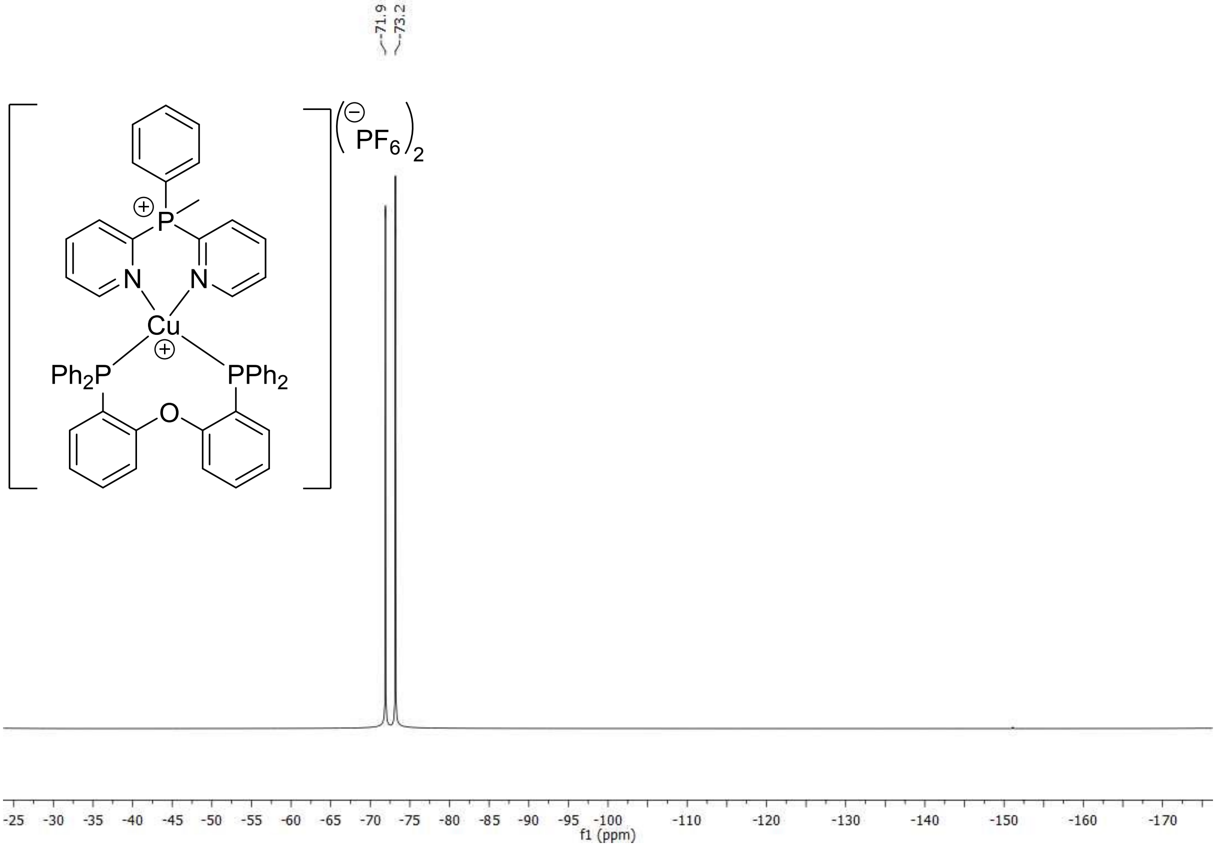

Figure S27: ^{19}F NMR (565MHz, acetone-*d$_6$*) spectrum of complex **5**.

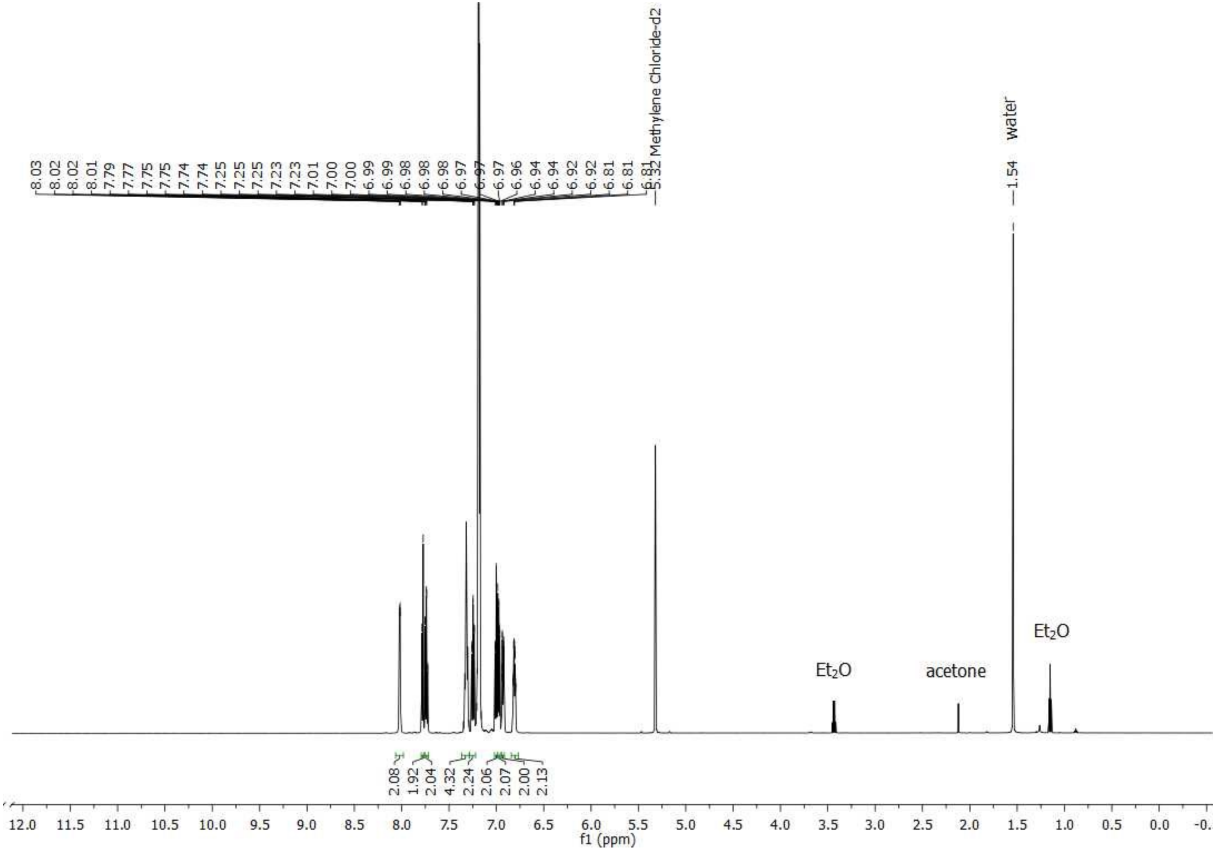

Figure S28: ^{1}H NMR (600 MHz, CD_2Cl_2) spectrum of complex **6**.

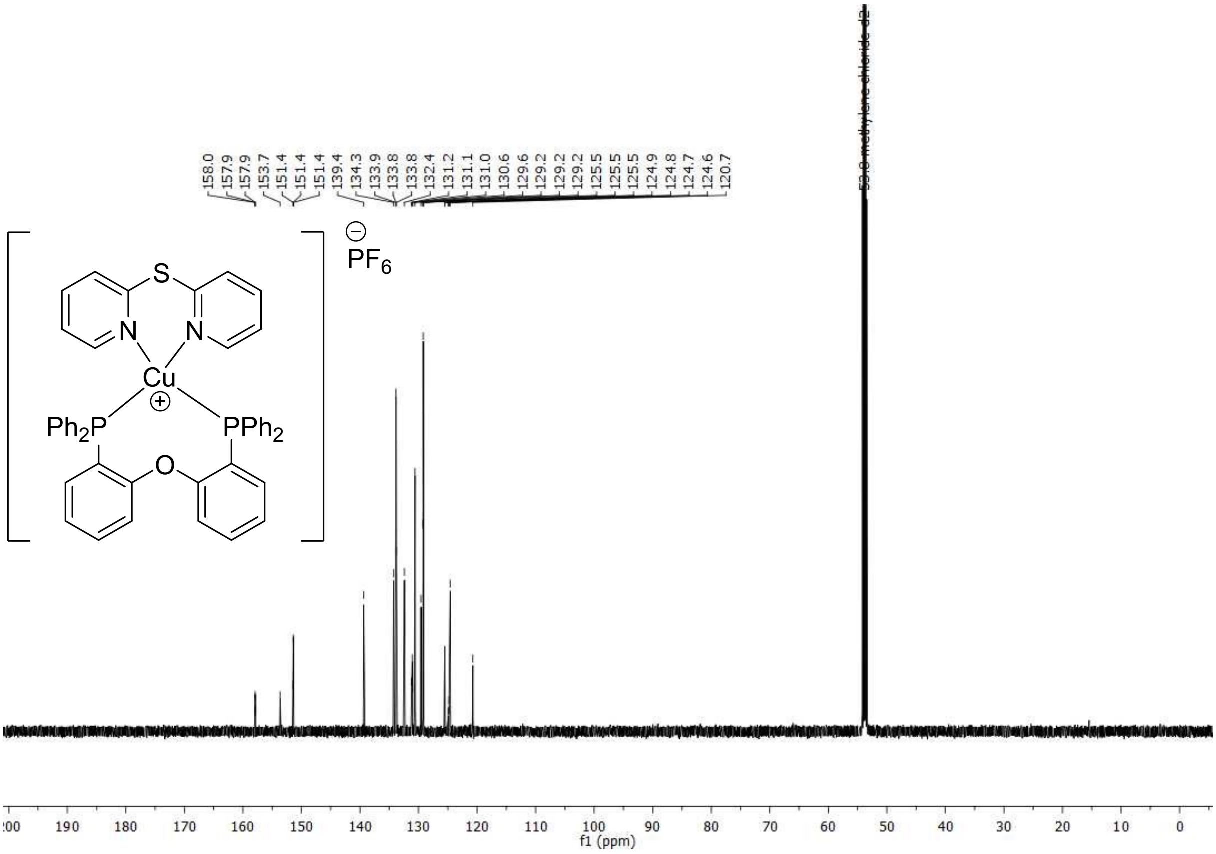

Figure S29: ^{13}C NMR (151 MHz, CD_2Cl_2) spectrum of complex **6**.

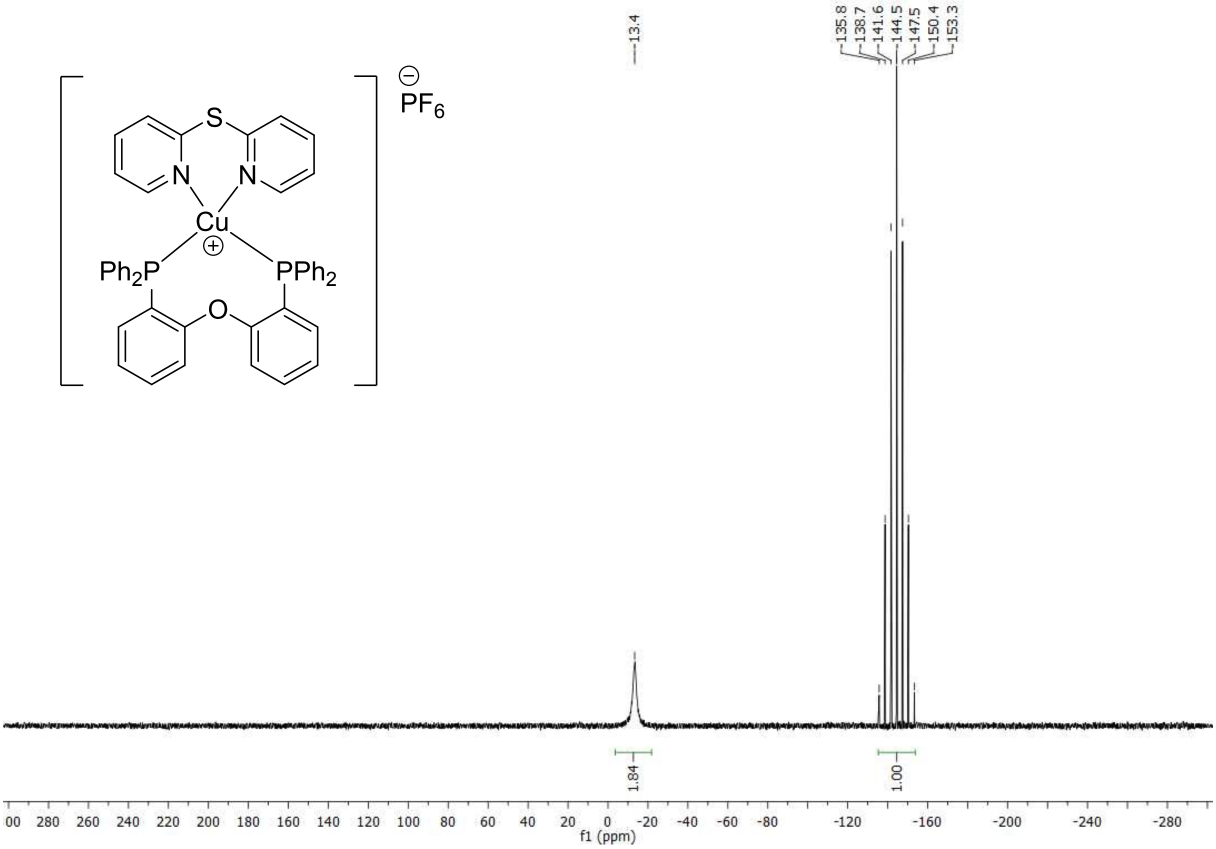

Figure S30. ^{31}P NMR (243 MHz, CD_2Cl_2) spectrum of complex **6**.

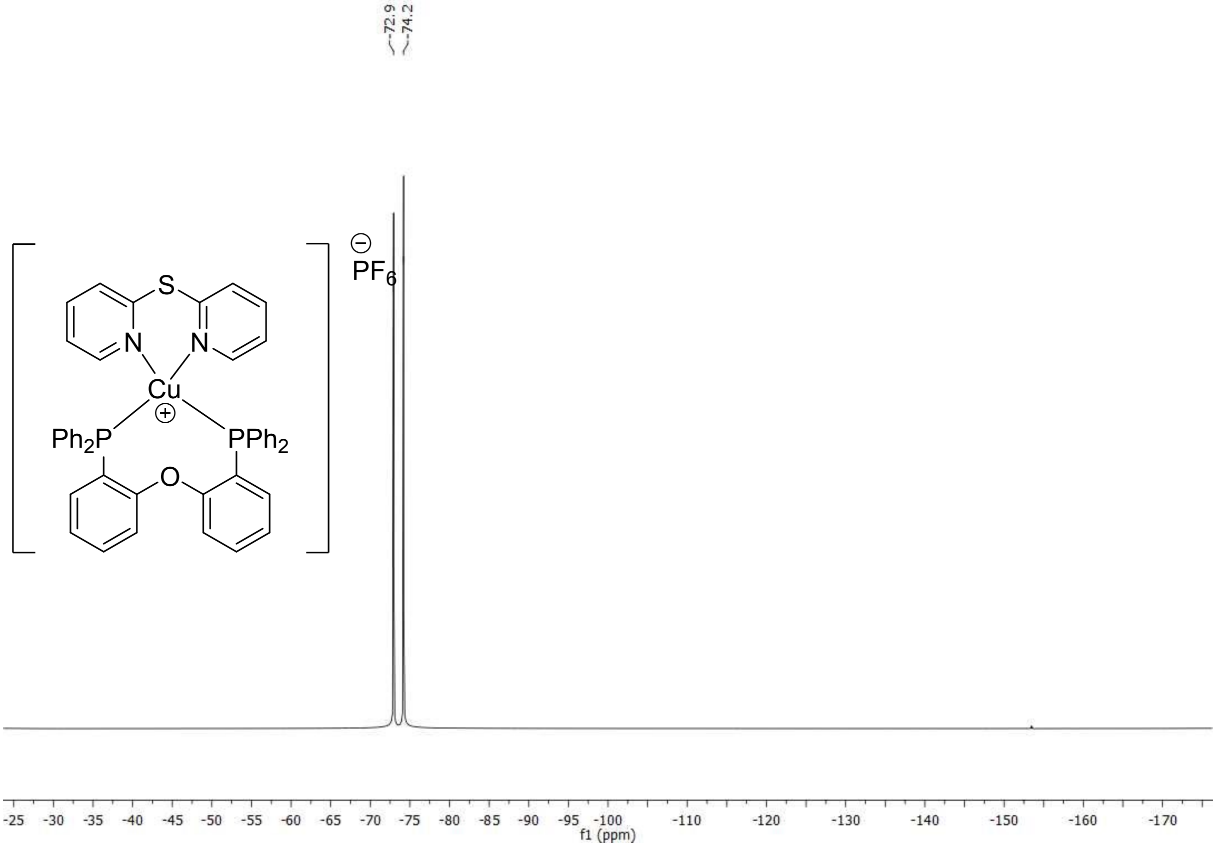

Figure S31. ^{19}F NMR (565 MHz, CD_2Cl_2) spectrum of complex **6**.

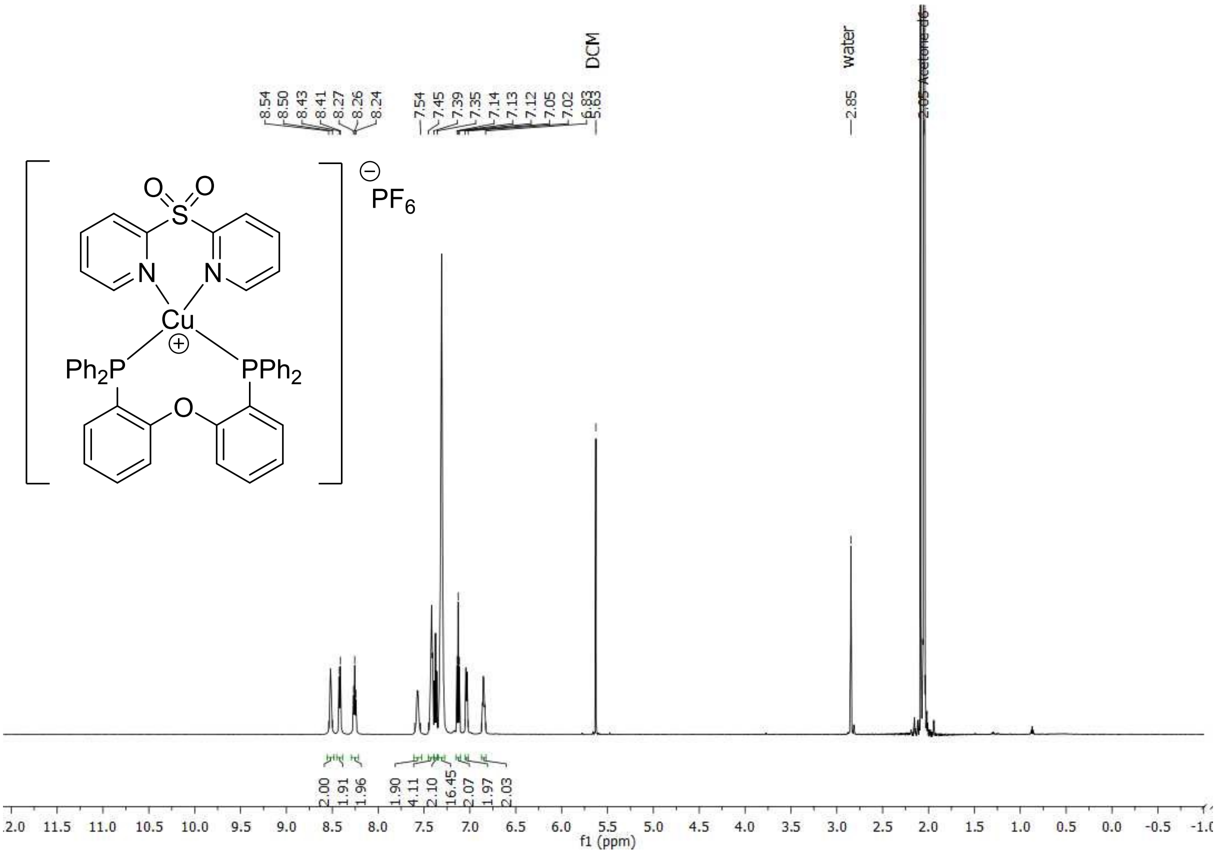

Figure S32. ^{1}H NMR (600MHz, acetone-d_6) spectrum of complex **7**.

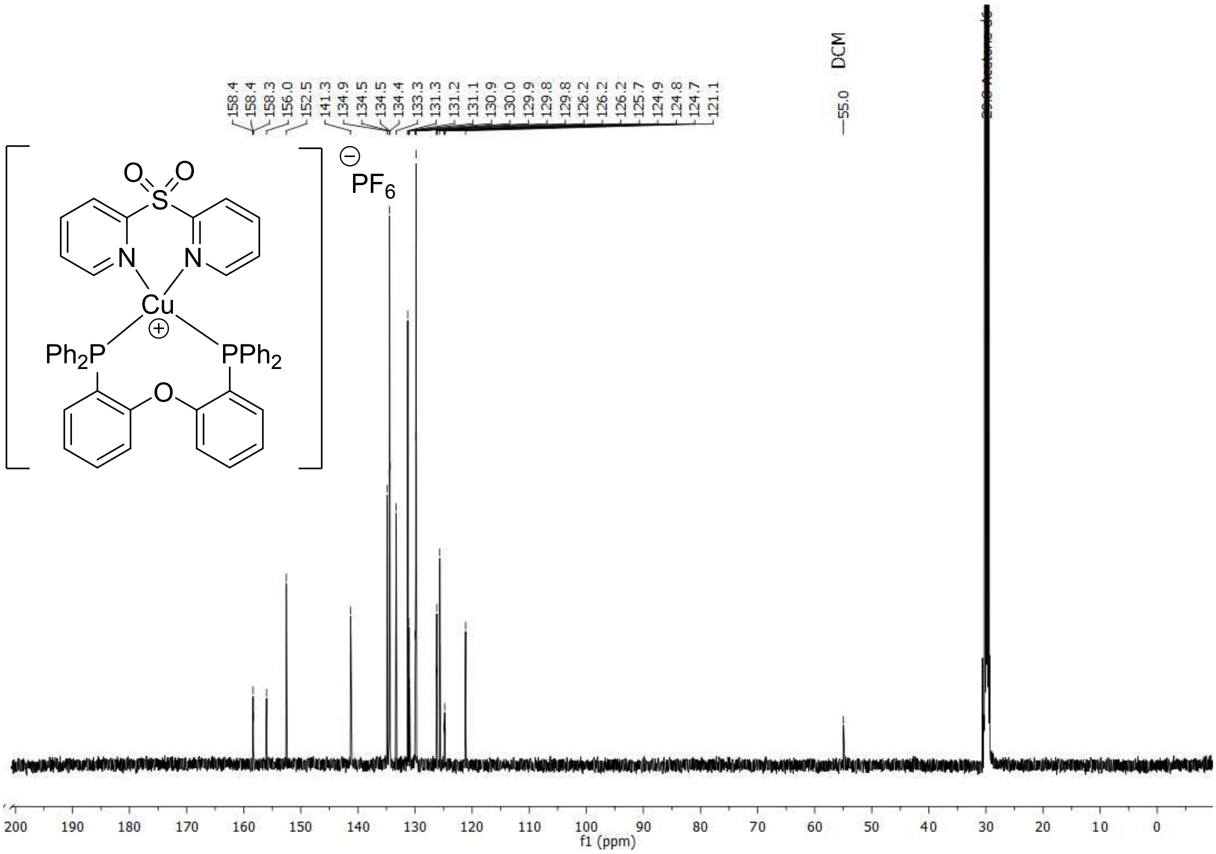

Figure S33. ^{13}C NMR (125 MHz, acetone-*d$_6$*) spectrum of complex **7**.

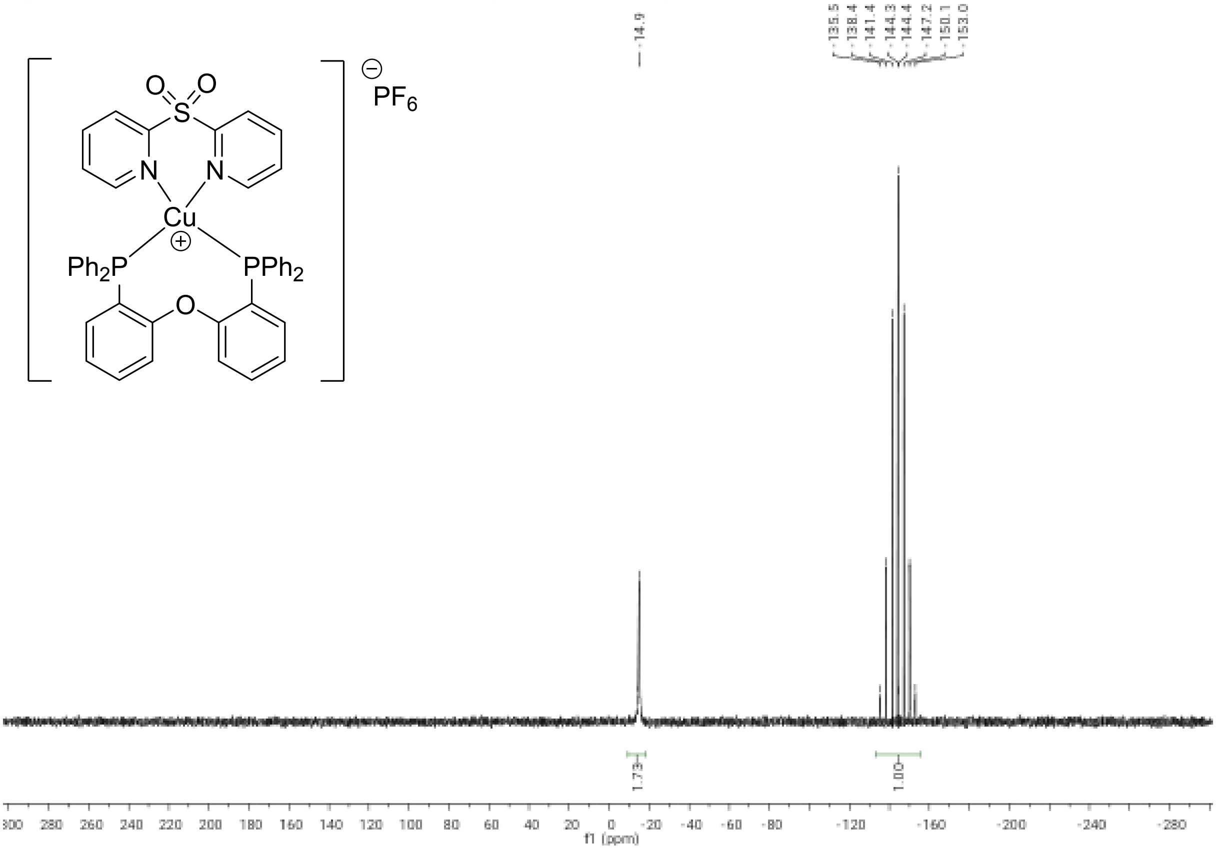

Figure S34. ^{31}P NMR (243 MHz, acetone-*d$_6$*) spectrum of complex **7**.

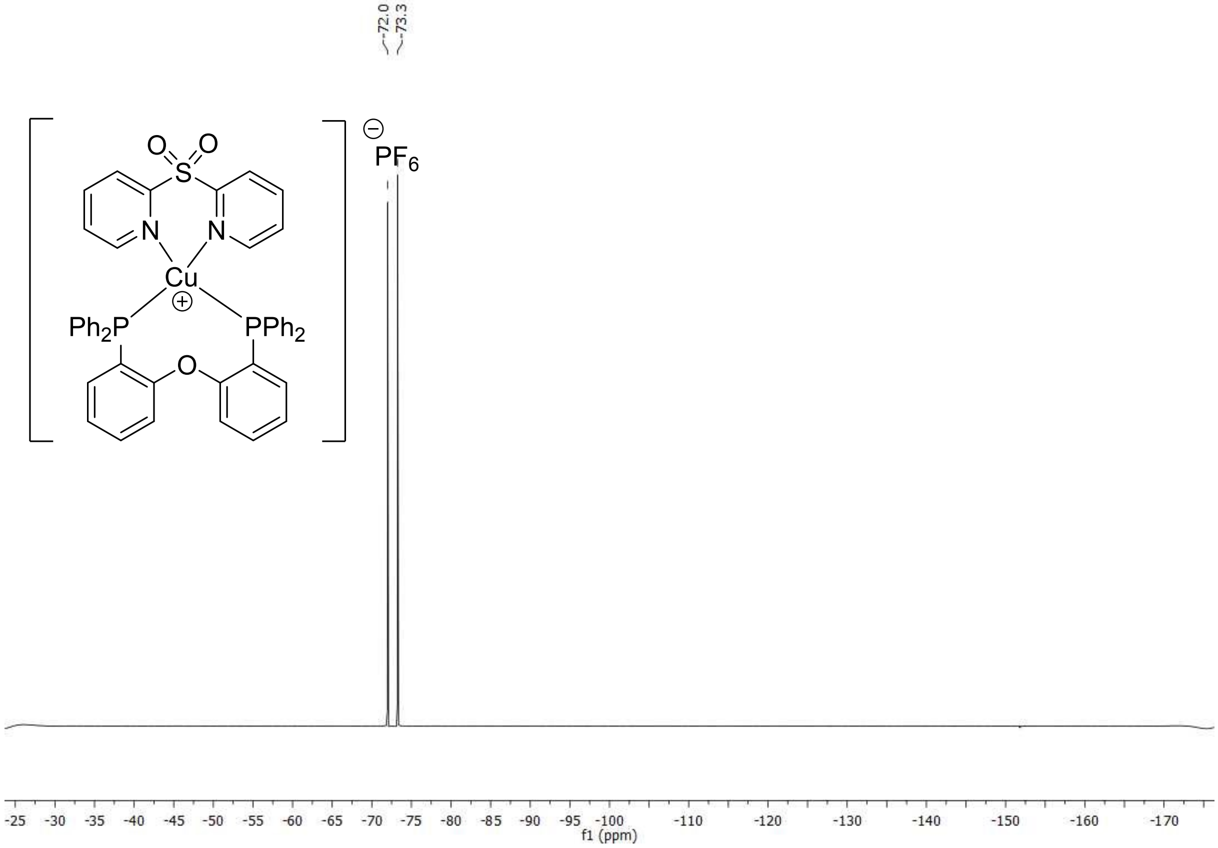

Figure S35. ^{19}F NMR (565 MHz, acetone-*d*$_6$) spectrum of complex **7**.

Determination of weak interactions in complexes **1**-**7**.

In **1**, only one intra-ligand π…π interaction has been detected in DPEPhos. This interaction occurred between one phenyl ring of one PPh_2 moiety and of one O-substituted aromatic ring, with a distance value of 3.7983(15) Å between both centroids.

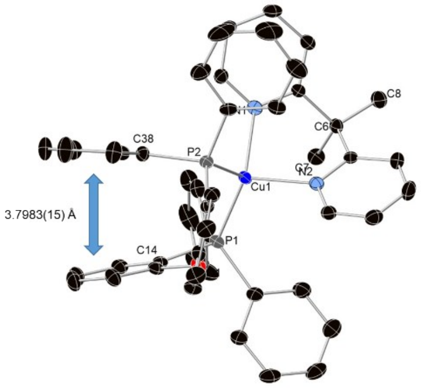

Figure S36. Weak interactions in **1**.

In **2**, two intra-ligand CH…π interactions were detected in the DPEPhos ligand. These interactions were between one hydrogen atom of one O-substituted aromatic ring and one P-substituted aromatic ring of DPEPhos, with values determined both at 2.99 Å. Noteworthy, an inter-ligand interaction between one hydrogen atom in alpha position of one pyridine ring of the N^N ligand and the oxygen atom of the DPEPhos was observed, with a distance value of 2.44 Å.

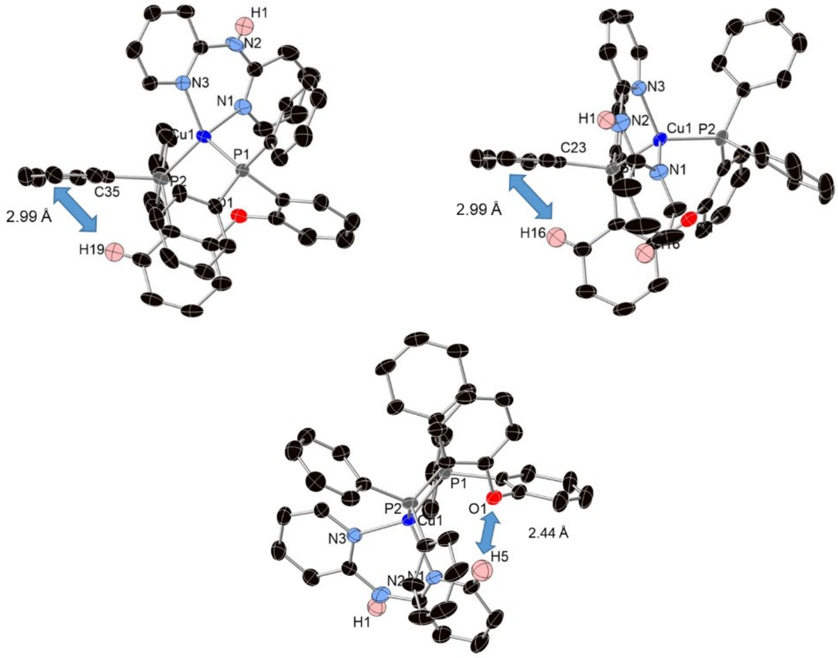

Figure S37. Weak interactions in **2**.

In **4**, three weak interactions were observed. One intra-ligand π…π interaction in DPEPhos like in **1**, with a distance value of 3.6779(14) Å between both centroids. The two others were CH…π interactions, one intra-ligand interaction as for **2**, with a distance value of 2.98 Å, and the second was an inter-ligand CH…π interaction between a hydrogen atom of P-substituted aromatic ring of DPEPhos and one pyridine ring of the N^N ligand, with a distance value of 2.98 Å.

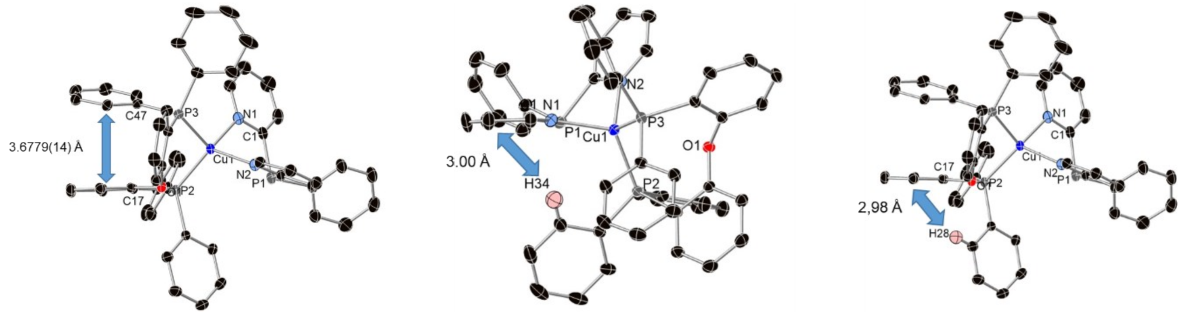

Figure S38. Weak interactions in **4**.

5 was the copper complex containing the biggest number of weak interactions, with a total of five. In details, two of them were π…π interactions, one intra-ligand between one phenyl ring of one PPh_2 moiety and of one O-substituted aromatic ring of DPEPhos (distance value of 3.720(4) Å), and one inter-ligand between one pyridine ring in the N^N ligand and one phenyl ring of one PPh_2 framework in DPEPhos (distance value of 4.073(6) Å). Then, two inter-ligand CH…π interactions have been noticed, one between one hydrogen atom of the phenyl ring of the phosphonium ligand and one phenyl ring of DPEPhos (distance value of 2.81 Å) and one between one hydrogen atom of the phenyl ring of the DPEPhos and the phenyl ring of the phosphonium ligand (distance value of 2.56 Å). Finally, like in **2**, an inter-ligand interaction between one hydrogen atom in alpha position of one pyridine ring of the N^N ligand and the oxygen atom of the DPEPhos was observed, with a distance value of 2.38 Å. **5** exhibits four intra-ligand weak interactions which was by far the highest number considering the series of **1**-**7**.

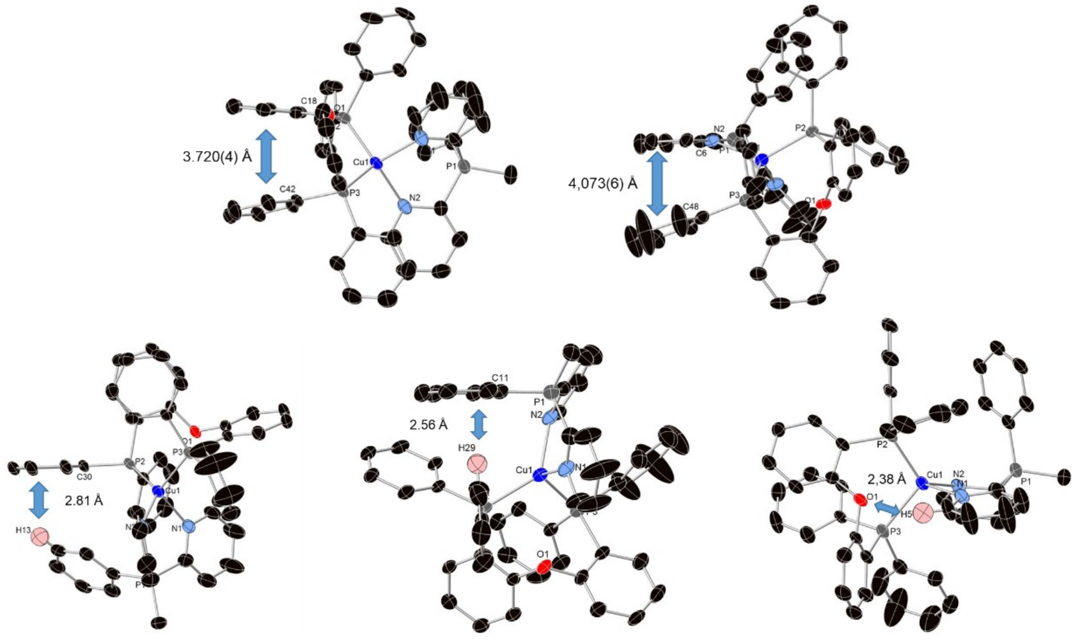

Figure S39. Weak interactions in **5**.

In **6**, one inter-ligand π…π interaction between one pyridine ring in the N^N ligand and one phenyl ring of one PPh_2 framework in DPEPhos (distance value of 3.7203(3) Å), and one intra-ligand interaction between one hydrogen atom of one phenyl ring of PPh_2 moiety and the oxygen atom of the DPEPhos (distance value of 2.34 Å), were observed.

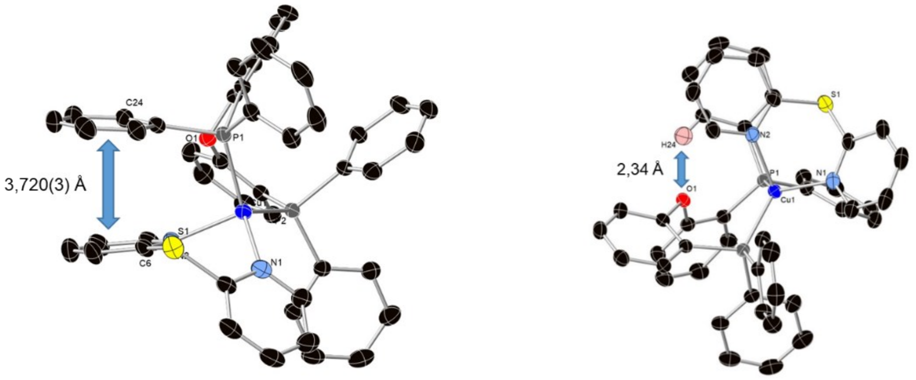

Figure S40. Weak interactions in **6**.

In **7**, two π…π interactions were observed. One intra-ligand π…π interaction between two phenyl rings in DPEPhos (distance value of 3.850(3) Å), and one inter-ligand π…π interaction between a pyridine ring of the N^N ligand and one phenyl ring of DPEPhos (distance value 3.748(4) Å) were detected.

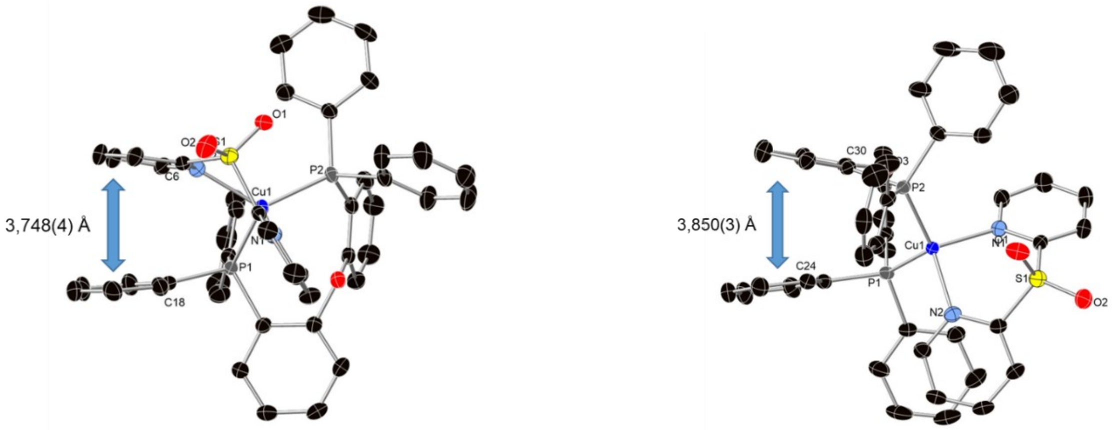

Figure S41. Weak interactions in **7**.

Table S1. Crystallographic data of complexes **1-4**.

	1	**2**	**3**	**4**
Chemical formula	$C_{49}H_{42}CuF_6N_2OP_3$	$C_{46}H_{37}CuF_6N_3OP_3$	$C_{46}H_{36}CuF_6N_2O_2P_3$	$C_{53}H_{43}Cl_2CuF_6N_2OP_4$
Mr	945.29	918.23	919.22	1096.21
Crystal system, space group	Triclinic, P$\underline{1}$	Triclinic, P$\underline{1}$	Triclinic, P$\underline{1}$	Triclinic, P$\underline{1}$
Temperature (K)	150	150	150	150
a, b, c (Å)	11.3068 (8), 13.913 (1) 14.5022 (10)	12.5672 (3), 13.8653 (3) 15.6258 (3)	12.4849 (4), 13.5940 (5), 14.4864 (5)	12.5814 (4), 13.2569 (4), 16.1401 (6)
β (°)	75.286 (4), 84.950 (4) 83.773 (4)	84.435 (1), 86.169 (1) 68.557 (1)	98.081 (1), 103.809 (1), 102.778 (1)	66.581 (1), 82.406 (1), 87.921 (1)
V (Å^3)	2189.2 (3)	2520.91 (10)	2279.38 (14)	2448.20 (14)
Z	2	2	2	2
Radiation type	Mo Kα	Mo Kα	Mo Kα	Mo Kα
μ (mm^{-1})	0.67	0.58	0.65	0.75
Crystal size (mm)	0.25 × 0.15 × 0.14	0.30 × 0.26 × 0.22	0.20 × 0.14 × 0.11	0.19 × 0.14 × 0.10
Data collection				
Diffractometer	Bruker APEX-II CCD	Bruker APEX-II CCD	Bruker APEX-II CCD	Bruker APEX-II CCD
Absorption correction	Multi-scan SADABS 2015/1	Multi-scan SADABS 2015/1	Multi-scan SADABS 2015/1	Multi-scan SADABS 2015/1
No. of measured, independent and observed [I > 2σ(I)] reflections	26809, 8372, 6409	38990, 10999, 9210	97639, 21992, 14943	120005, 27457, 16384
R$_{int}$	0.046	0.022	0.061	0.085
(sin θ/λ)max (Å^{-1})	0.617	0.641	0.833	0.878
Refinement				
R[F^2 > 2σ(F^2)], wR(F^2), S	0.037, 0.090, 1.05	0.049, 0.158, 1.12	0.045, 0.126, 1.09	0.073, 0.239, 1.04
No. of reflections	8372	10999	21992	27457
No. of parameters	561	545	541	622
H-atom treatment	H-atom parameters constrained	H atoms treated by a mixture of independent and constrained refinement	H-atom parameters constrained	H-atom parameters constrained
Δ$_{pmax}$, Δ$_{pmin}$ (e Å^{-3})	0.40, –0.47	0.92, –0.49	0.52, −0.92	2.81, −2.80

Table S2. Crystallographic data of complexes **5-7.**

	5		**6**	7
Chemical formula	$C_{53}H_{44}CuN_2OP_3 \cdot 2(F_6P)$		$C_{47}H_{38}Cl_2CuF_6N_2OP_3S$	$C_{46}H_{36}CuF_6N_2O_3P_3S$
Mr	1171.29		1020.20	967.28
Crystal system, space group	Triclinic, $P\underline{1}$		Triclinic, $P\underline{1}$	Triclinic, $P\underline{1}$
Temperature (K)	150		150	150
a, b, c (Å)	12.1423 (11), 12.7994 (11), 21.433 (2)		12.1153 (7), 12.4627 (7), 16.4049 (9)	12.0630 (6), 13.2432 (7), 15.9305 (8)
β (°)	73.615 (4), 87.899 (4), 63.330 (3)		75.887 (2), 89.566 (2), 68.532 (2)	96.067 (2), 111.521 (2), 93.100 (2)
V ($Å^3$)	2839.9 (5)		2226.4 (2)	2342.4 (2)
Z	2		2	2
Radiation type	Mo Kα		Mo Kα	Mo Kα
μ (mm^{-1})	0.60		0.83	0.68
Crystal size (mm)	0.17 × 0.07 × 0.02		0.21 × 0.16 × 0.05	0.20 × 0.12 × 0.08
Data collection				
Diffractometer	Bruker APEX-II CCD		Bruker APEX-II CCD	Bruker D8QUEST
Absorption correction	Multi-scanSADABS 2015/1		Multi-scan SADABS 2015/1	Multi-scan SADABS 2016/1
No. of measured, independent and observed [I > 2σ(I)] reflections	70012, 14275, 11375		77399, 13006, 9826	70012, 14275, 11375
R_{int}	0.045		0.062	0.045
(sin θ/λ)max ($Å^{-1}$)	0.715		0.705	0.715
Refinement				
$R[F^2 > 2\sigma(F^2)]$, $wR(F^2)$, S	0.038, 0.096, 1.08		0.058, 0.164, 1.04	0.038, 0.096, 1.08
No. of reflections	14275		13006	14275
No. of parameters	596		568	596
H-atom treatment	H-atom parameters constrained		H-atom parameters constrained	H-atom parameters constrained
$\Delta_{\rho max}$, $\Delta_{\rho min}$ (e $Å^{-3}$)	0.56, −0.45		1.47, −1.12	0.56, −0.45

Cyclic Voltammetry of complexes **1**-**7**

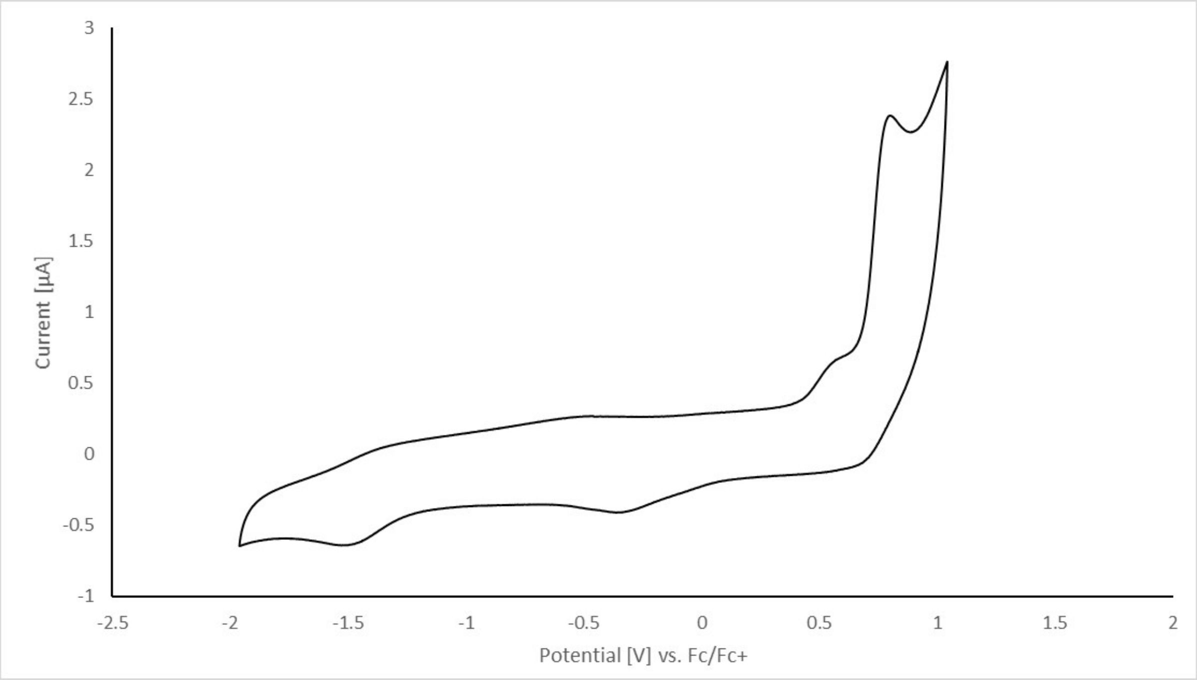

Figure S42. Cyclic Voltammetry of compound **1** vs (Fc/Fc+) at a scan rate of 0.1 V/s under nitrogen atmosphere.

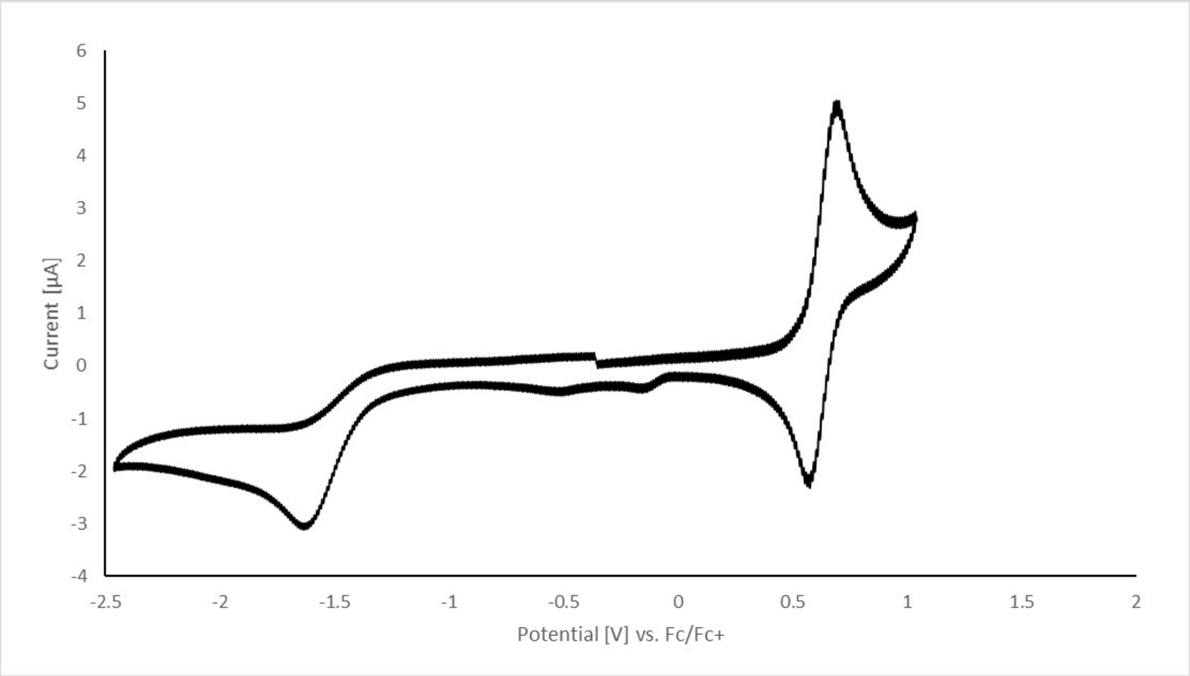

Figure S43. Cyclic Voltammetry of compound **2** vs (Fc/Fc+) at a scan rate of 0.1 V/s under nitrogen atmosphere.

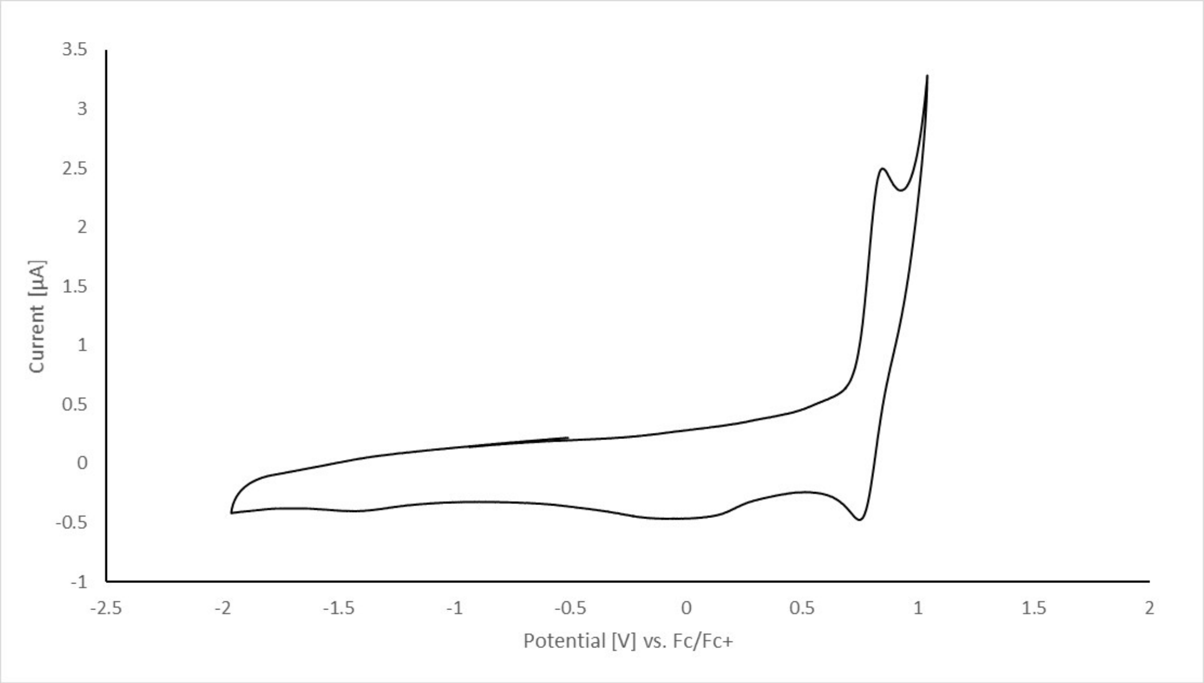

Figure S44. Cyclic Voltammetry of compound **3** vs (Fc/Fc+) at a scan rate of 0.1 V/s under nitrogen atmosphere.

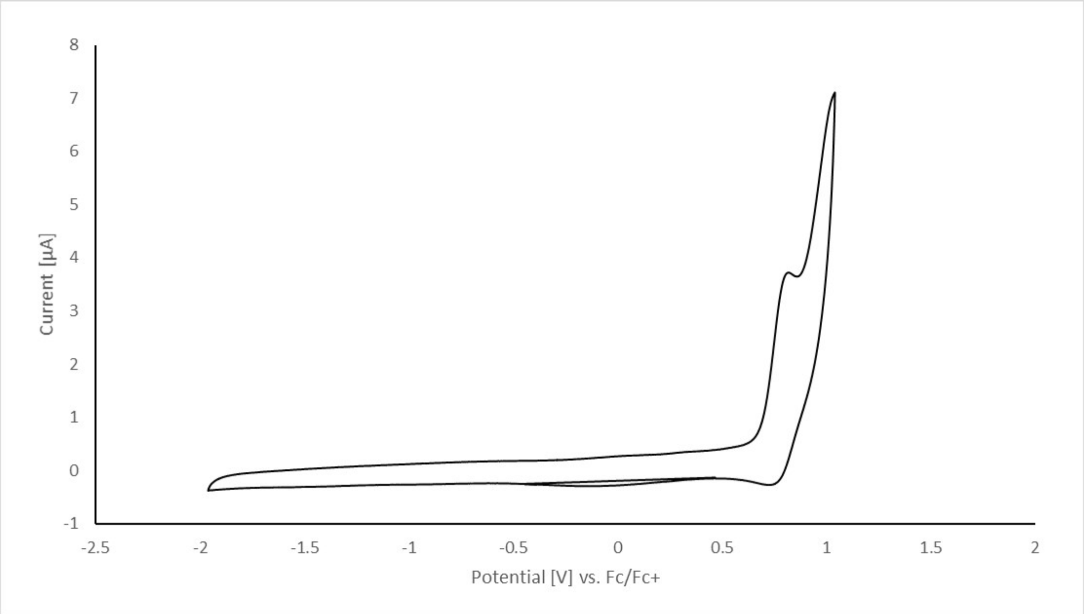

Figure S45. Cyclic Voltammetry of compound **4** vs (Fc/Fc+) at a scan rate of 0.1 V/s under nitrogen atmosphere.

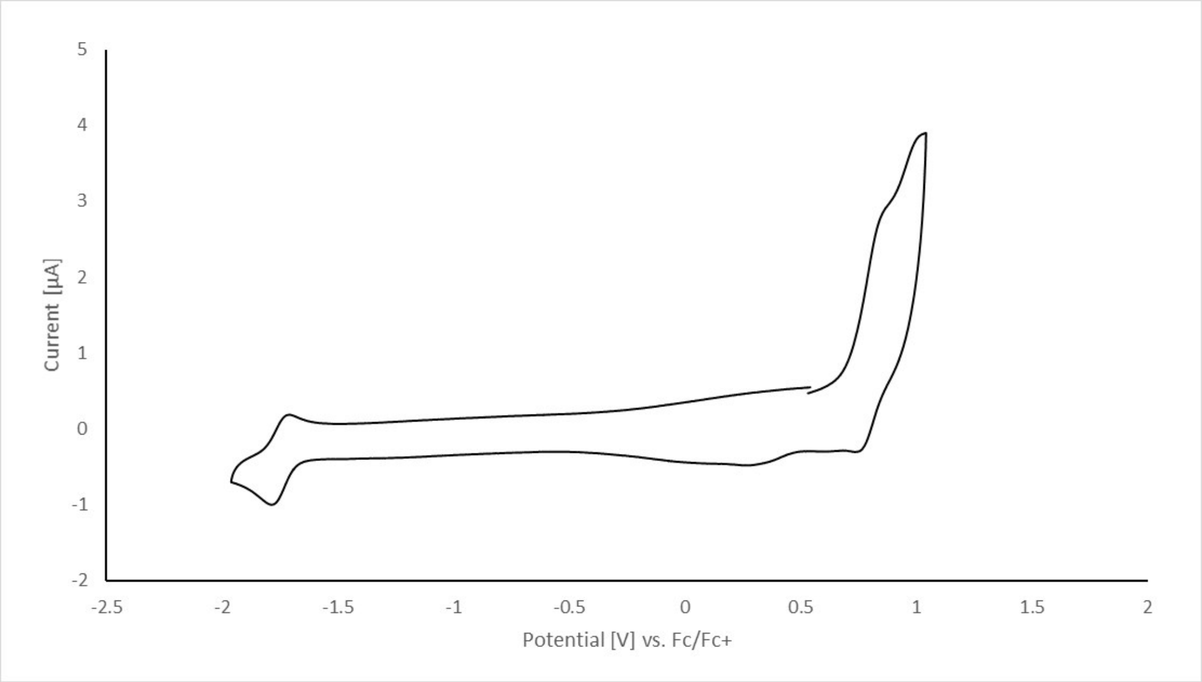

Figure S46. Cyclic Voltammetry of compound **5** vs (Fc/Fc+) at a scan rate of 0.1 V/s under nitrogen atmosphere.

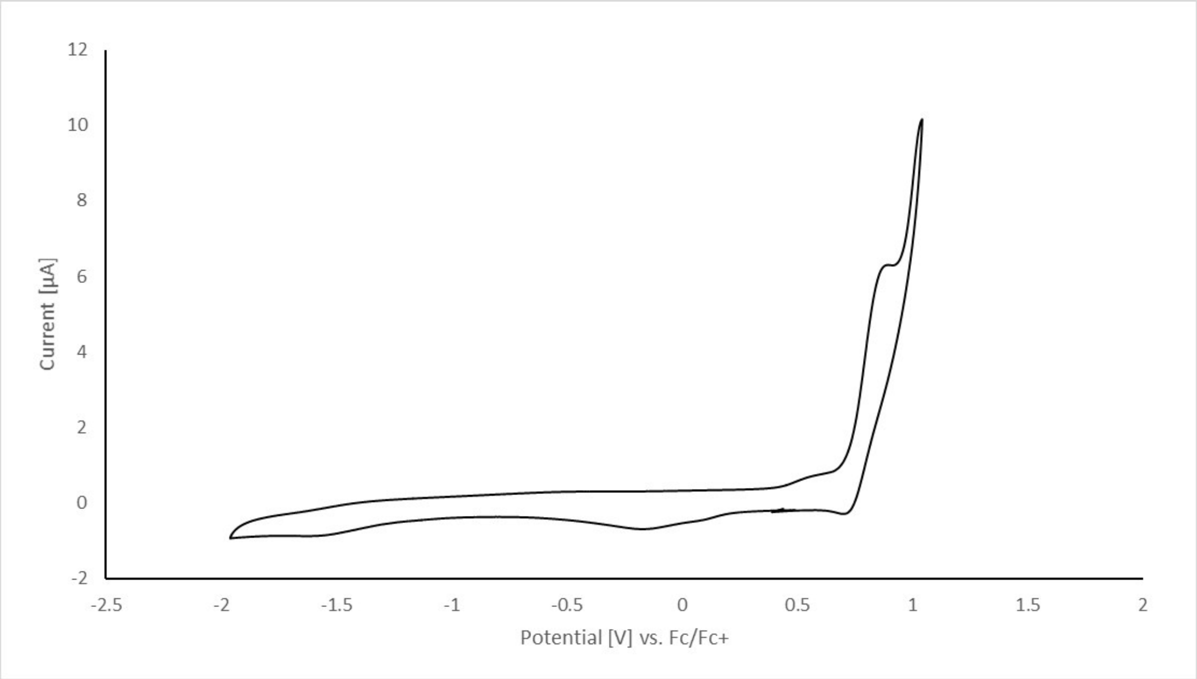

Figure S47. Cyclic Voltammetry of compound **6** vs (Fc/Fc+) at a scan rate of 0.1 V/s under nitrogen atmosphere.

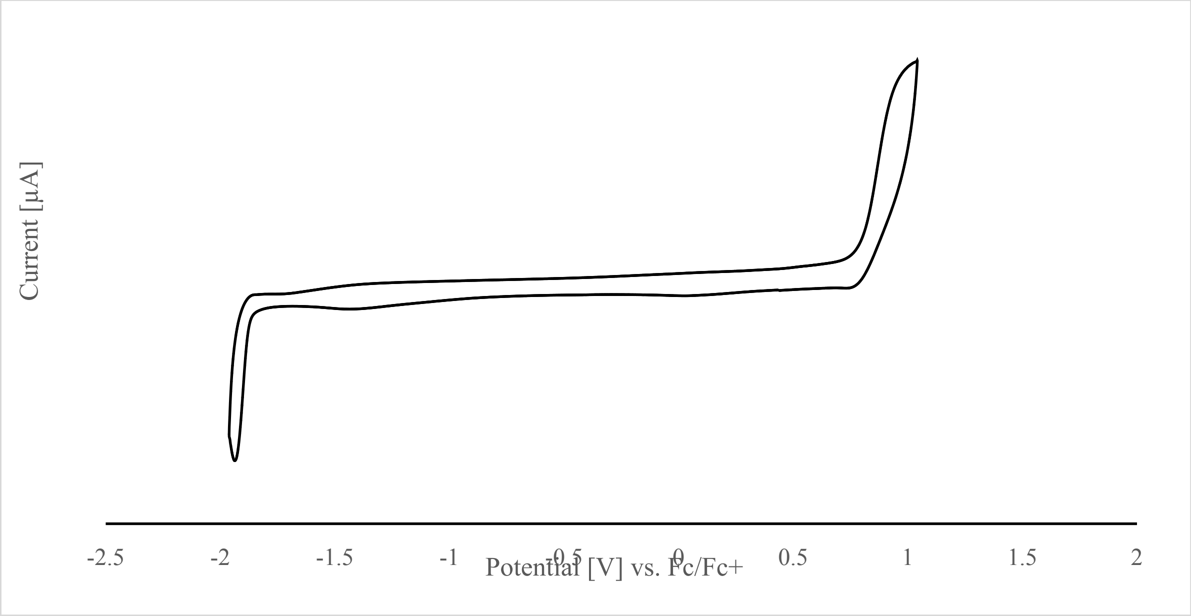

Figure S48. Cyclic Voltammetry of compound **7** vs (Fc/Fc+) at a scan rate of 0.1 V/s under nitrogen atmosphere.

Theoretically and experimentally photophysical characterization

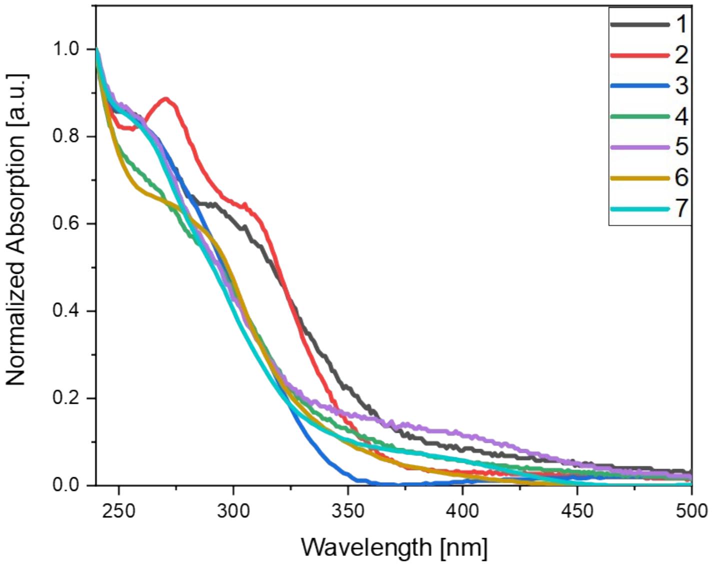

Figure S49. UV-Vis absorption of **1**-**7** in thin films onto a quartz substrate.

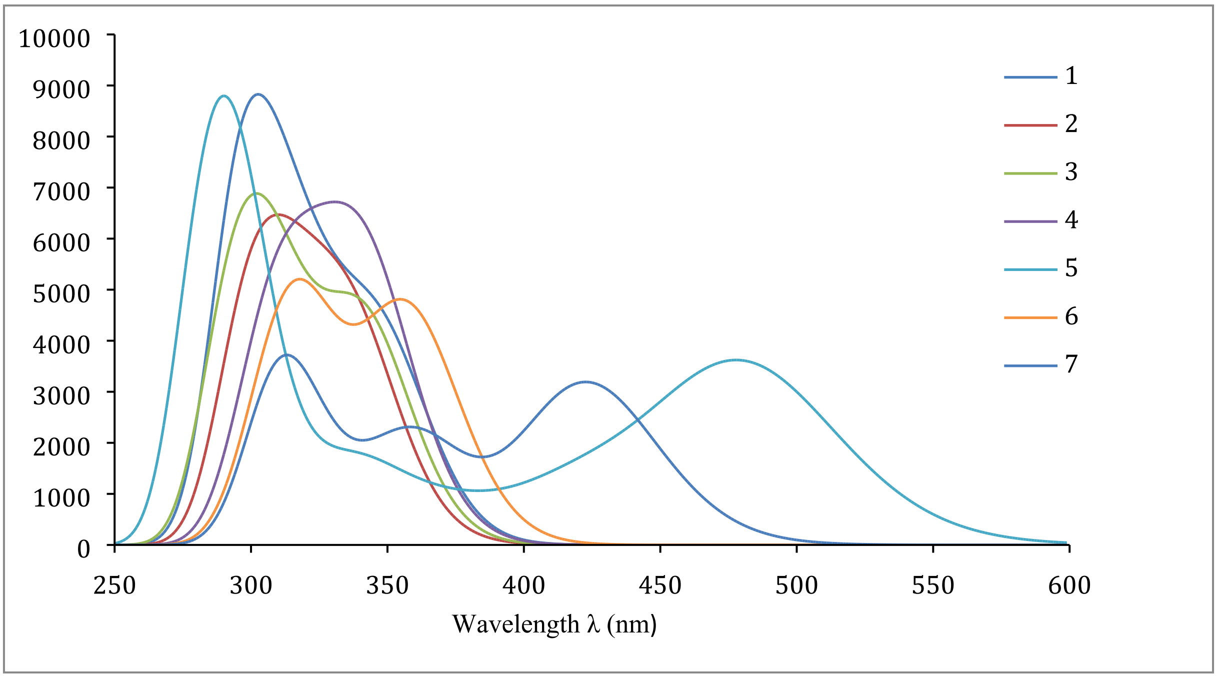

Figure S50. Calculated absorption spectra for the first 10 excited states for **1**-**7**.

Table S3. Calculated vertical transition energies (E), absorption wavelength (λ), and corresponding main MO description for the S_0->S_1 excitation for complexes **1**-**7**.

Complex	E (eV)	λ (nm)	Main MO contribution		Type
1	3.558	348.5	H->L	97%	ML-CT
2	3.387	366.1	H->L	98%	ML-CT
3	3.569	347.4	H->L H->L+1	70% 28%	ML-CT
4	3.623	342.2	H->L	96%	ML-CT
5	2.570	482.4	H->L	98%	ML-CT
6	3.400	364.7	H->L	95%	ML-CT
7	2.928	423.4	H->L	95%	ML-CT

Table S4. Theoretical $\Delta(S_1\text{->}S_0)$, $\Delta(T_1\text{->}S_0)$ and $\Delta E^{S\text{->}T}$ of **1-7** complexes.

Complex	$\Delta(S_1\text{->}S_0)$	$\Delta(T_1\text{->}S_0)$	$\Delta E^{S\text{->}T}$
1	1.80	1.63	0.16
2	2.24	2.15	0.10
3	2.01	1.88	0.12
4	1.81	1.66	0.18
5	2.00	1.80	0.05
6	1.25	1.23	0.09
7	0.91	0.74	0.09

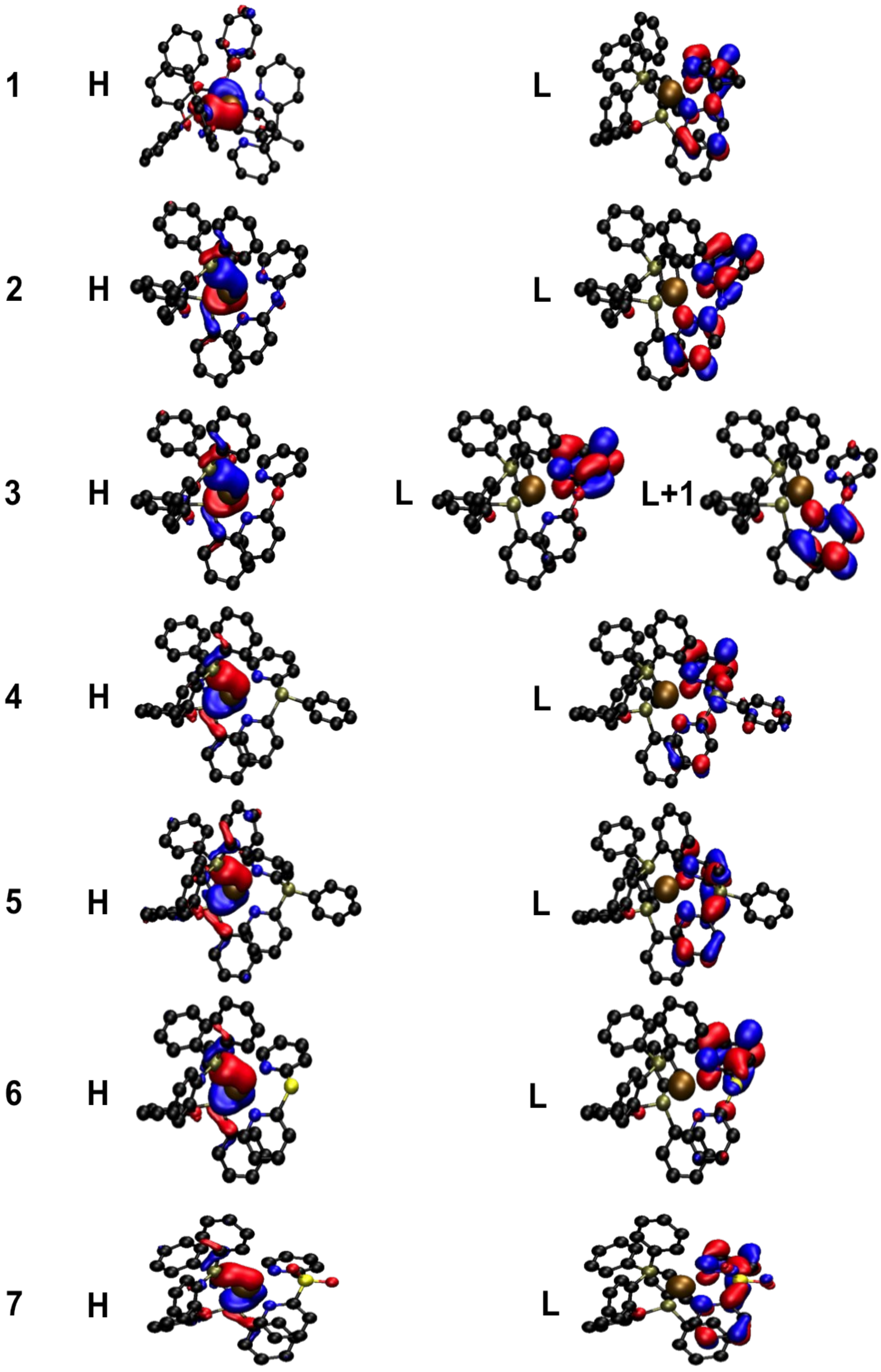

Figure S51. Frontier orbitals of the complexes relevant for the first excited states. H (HOMO), L (LUMO), L+1(LUMO+1).

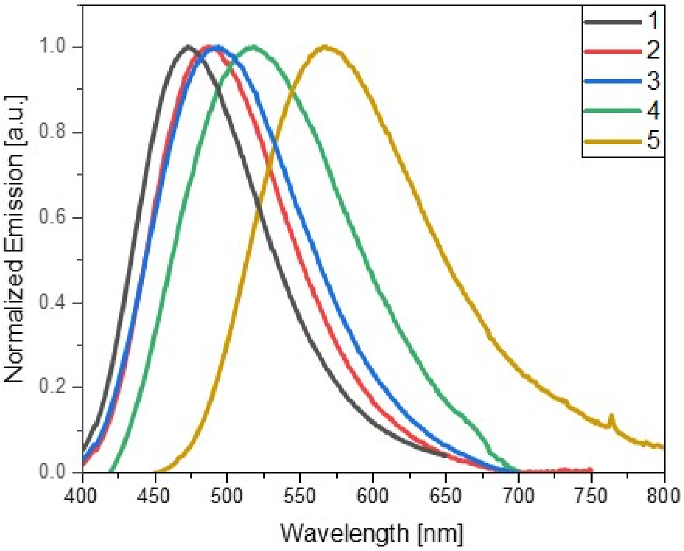

Figure S52. Normalized emission of **1-5** in DCM solution (left), and in thin films (right).

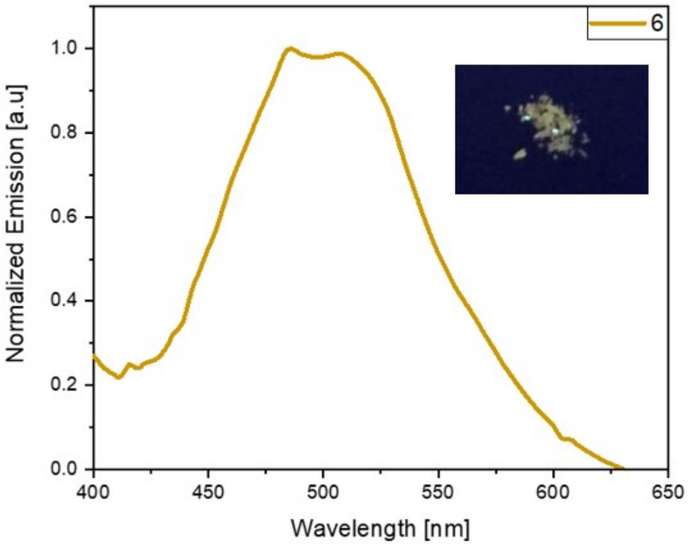

Figure S53. Emission spectra of complex **6** in crystal powder at RT. Inset: a picture of the powder under UV light (365 nm).

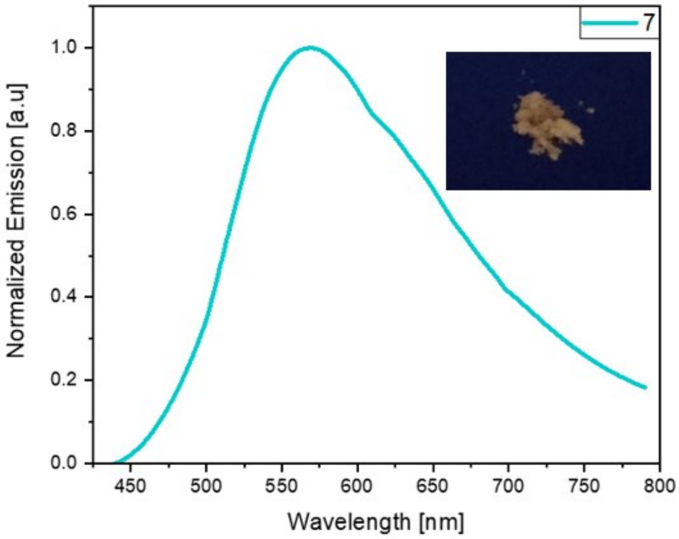

Figure S54. Emission spectra of complex **7** in crystal powder at RT. Inset: a picture of the powder under UV light (365 nm).

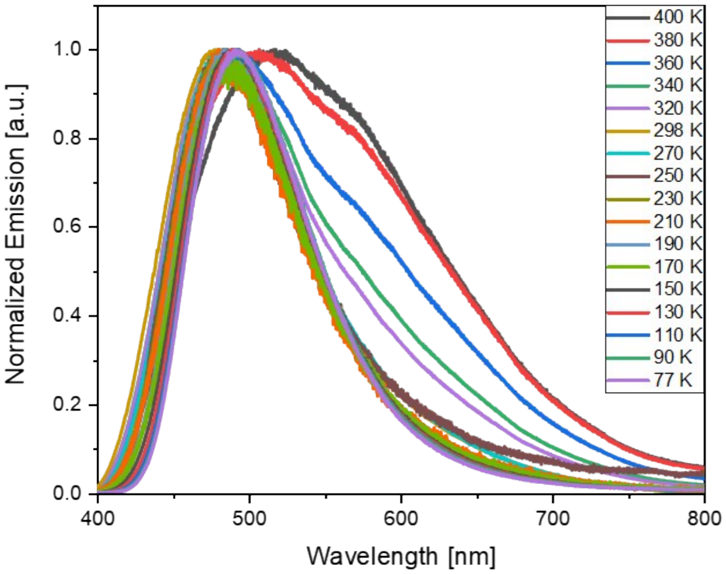

Figure S55. Emission spectra of **4** in crystalline powder at different temperatures ranging from 77 to 400 K (see legend).

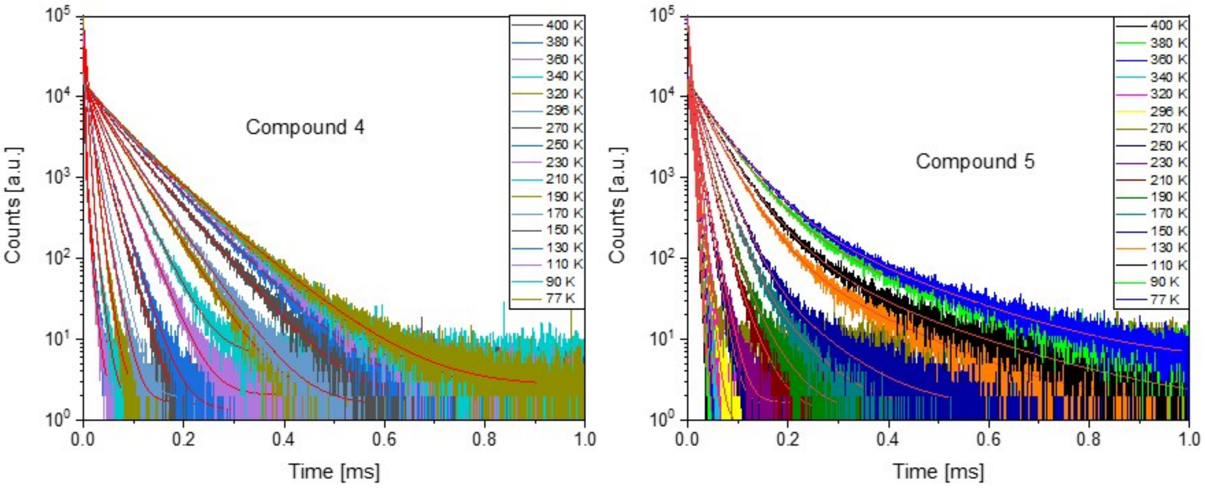

Figure S56. Excited-state lifetimes of **4** and **5** upon changing temperature.

Device characterization

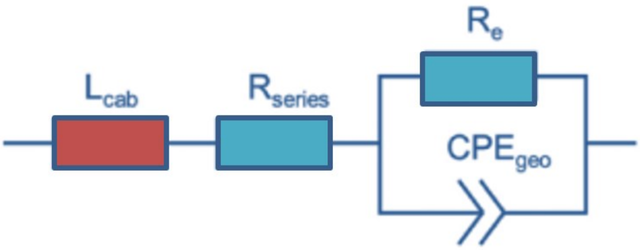

Figure S57. Simplified static EIS circuit model for LECs with electrical resistance (R_{LEC}) and constant phase element CPE_{geo}. A series resistor (R_{series}) and an inductor element for the cables (L_{cables}) were also included.

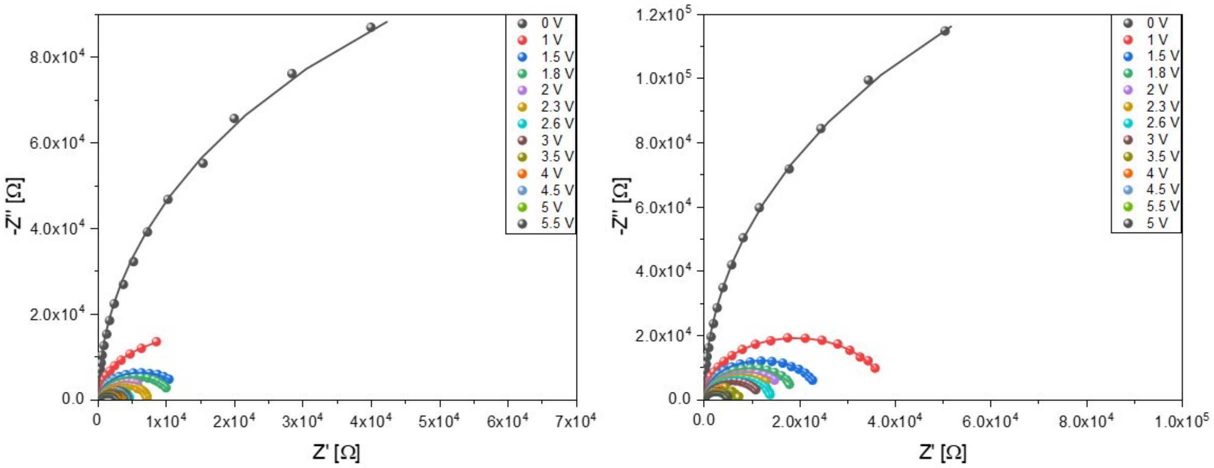

Figure S58. Nyquist plots of devices with **1** (left) and **2** (right) measured at different voltages (see legend).

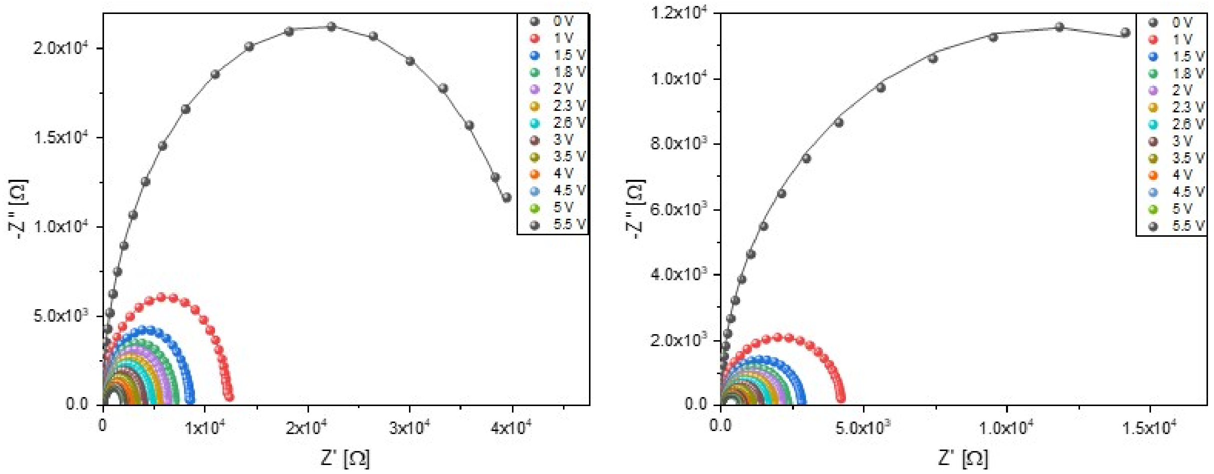

Figure S59. Nyquist plots of devices with **3** (left) and **4**(right) measured at different voltages (see legend).

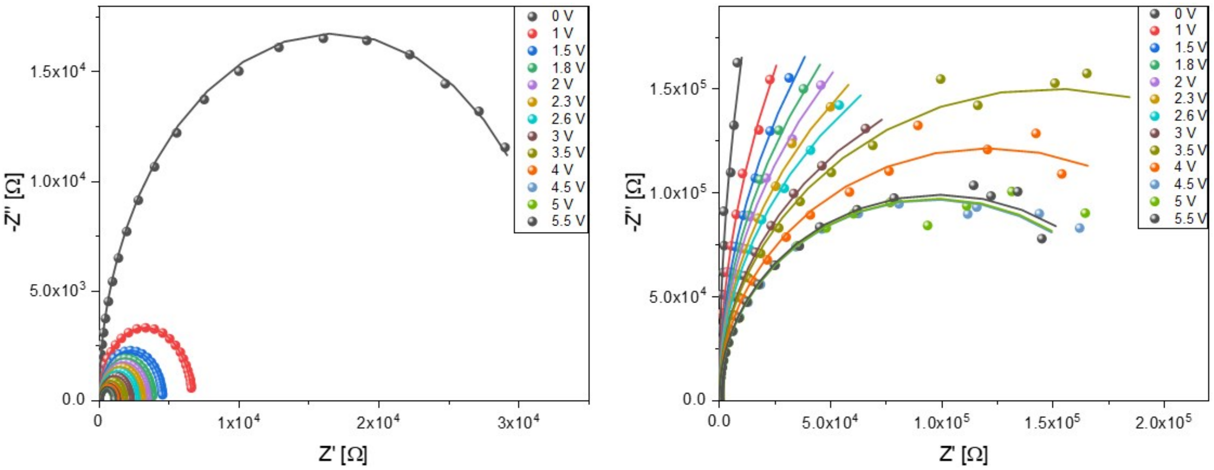

Figure S60. Nyquist plots of devices with **5** (left) and **6** (right) measured at different voltages (see legend).

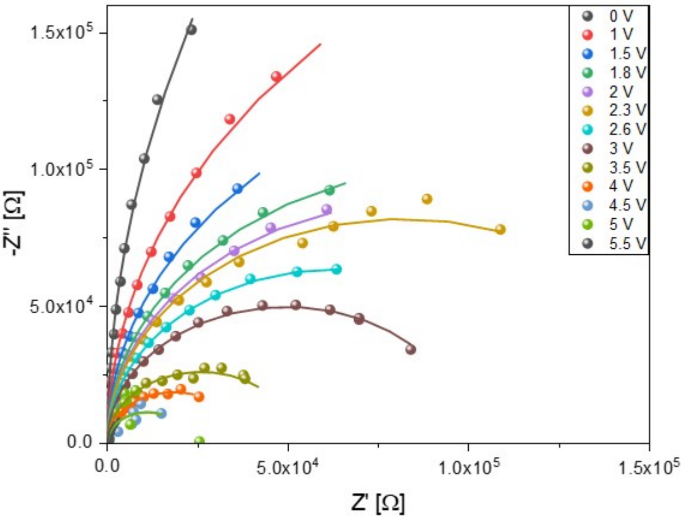

Figure S61. Nyquist plots of devices with **7** measured at different voltages (see legend).

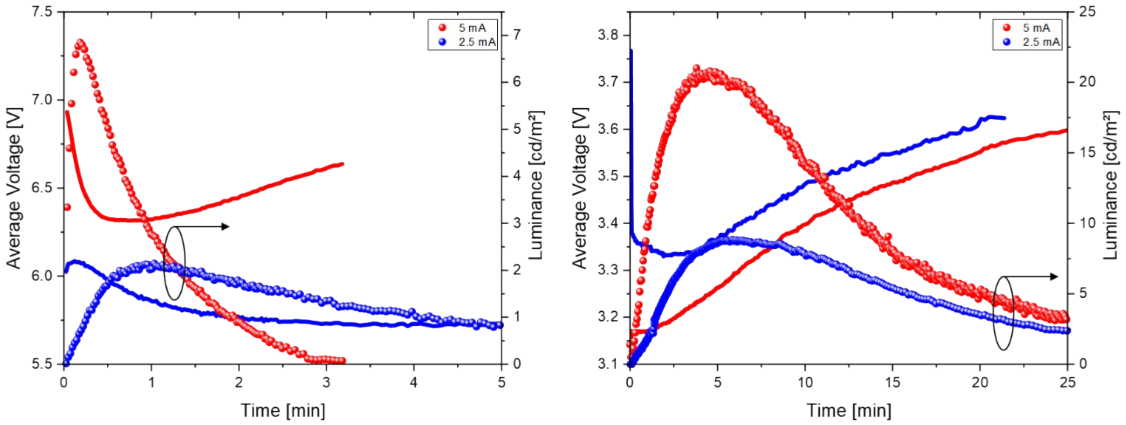

Figure S62. Average voltage and luminance over time of devices with **4** (left) and **5** (right) run at pulsed I_{av} 2.5 and 5 mA.

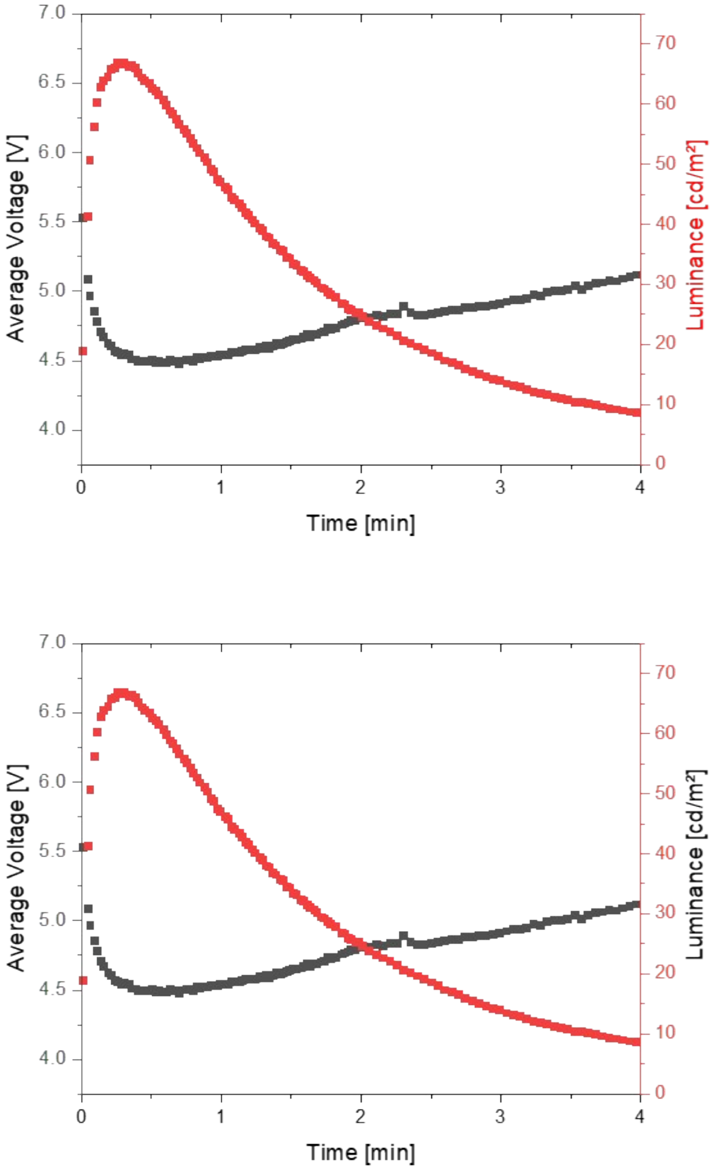

Figure S63. Average voltage (black) and luminance (red) over time of devices with CBP/**5** run at I_{av} 5 mA.

Thin film morphologies prepared with complexes **1**-**7**

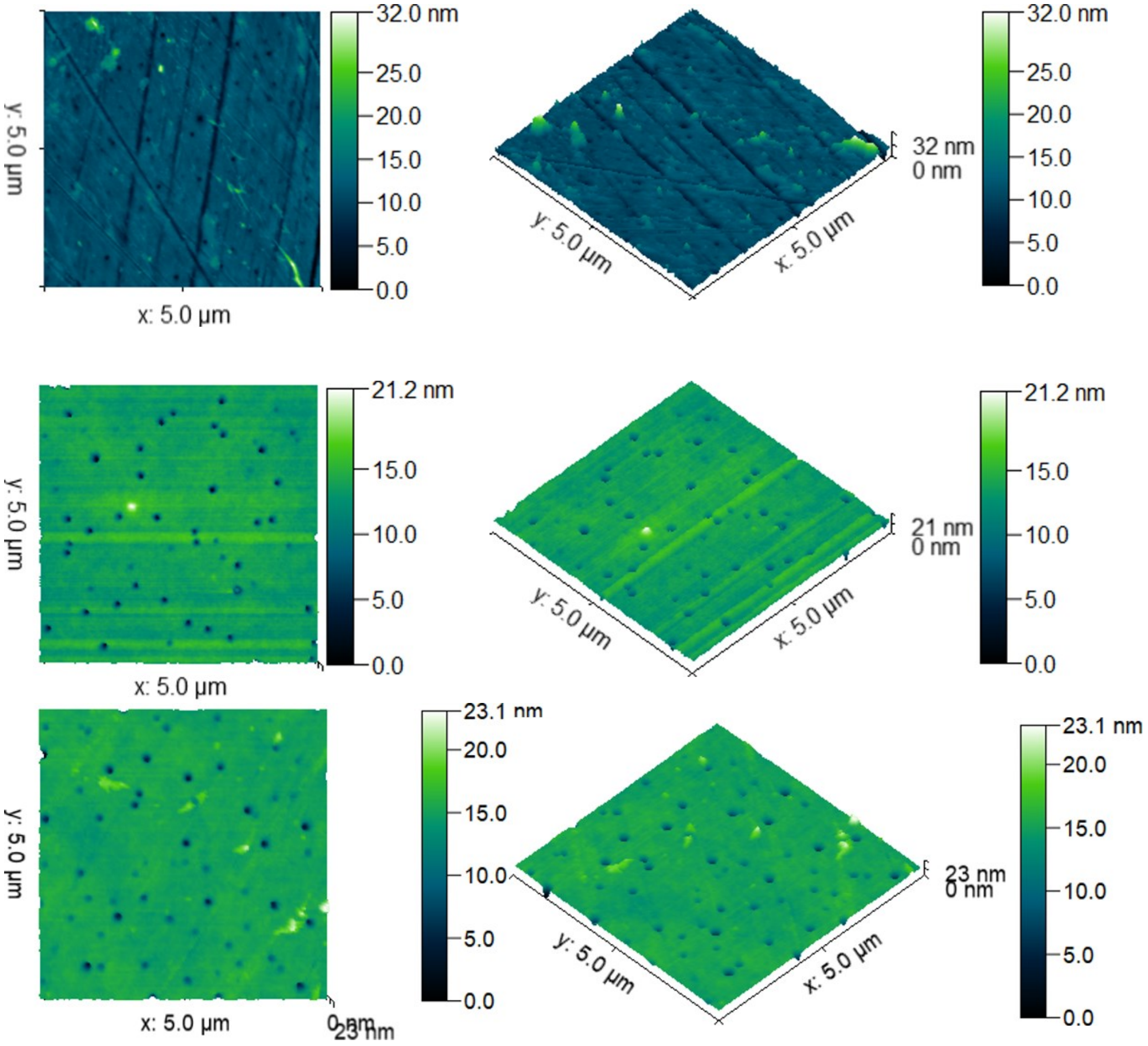

Figure S64. AFM image of **1** (top), **2** (centre), and **3** (bottom) thin films (5 x 5 µm).

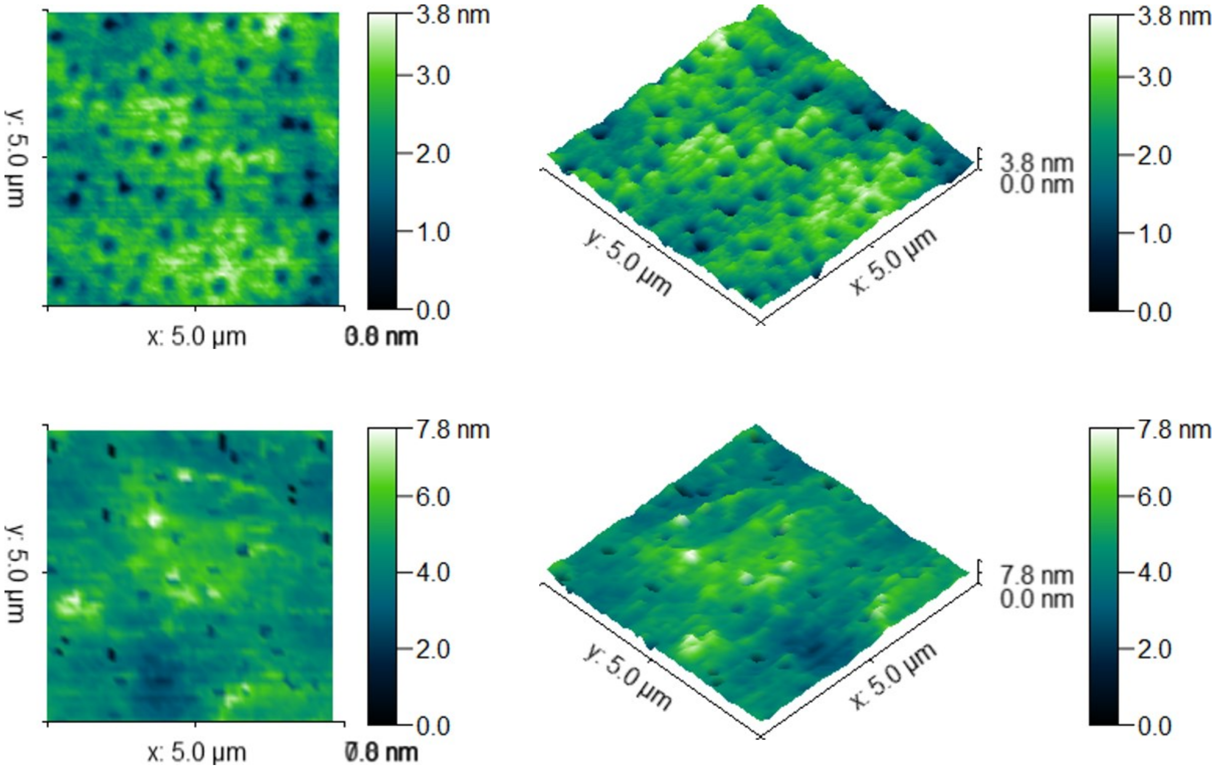

Figure S65. AFM image of **4** (top) and **5** (bottom) thin films (5 x 5 µm).

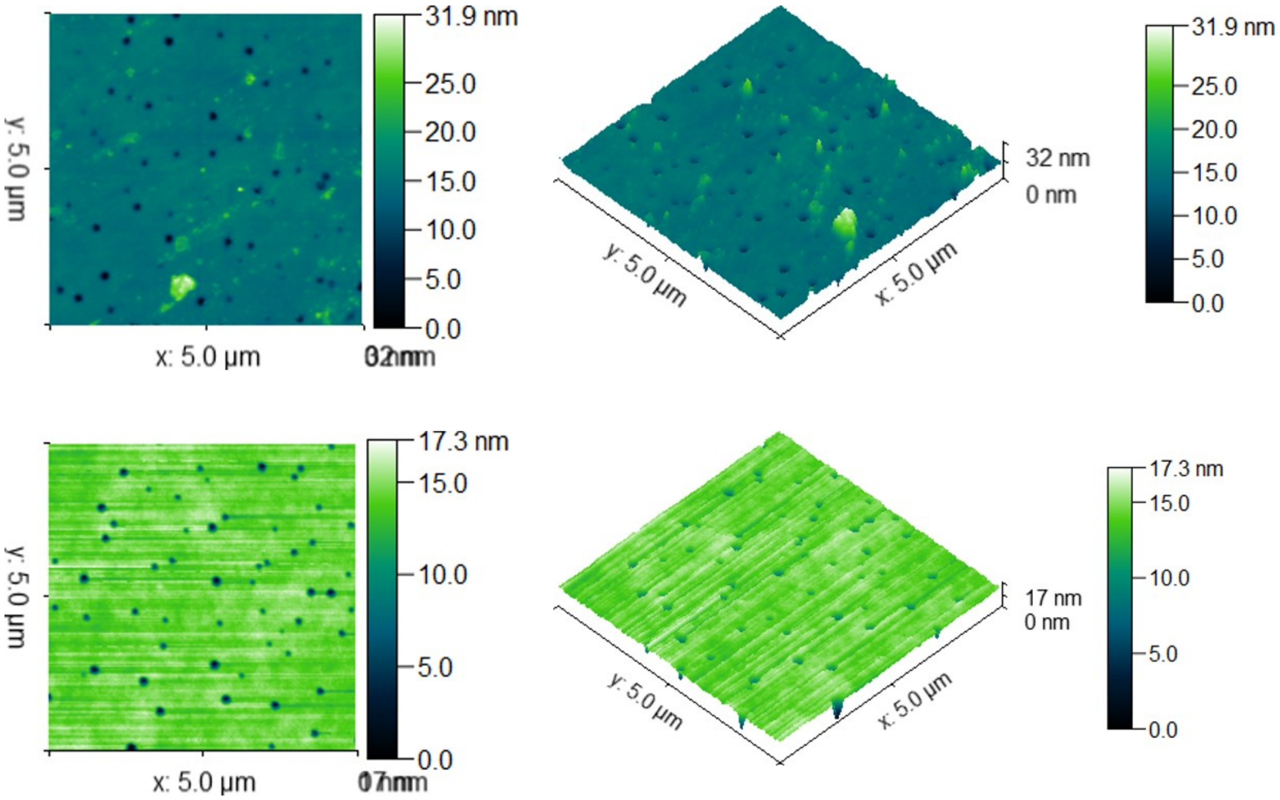

Figure S66. AFM image of **6** (top) and **7** (bottom) thin films (5 x 5 µm).

References

1 N. Vedernikov, R. Miftakhov, S. V. Borisoglebski, K. G. Caulton and B. N. Solomonov, *Chem. Heterocycl. Compd.*, 2002, **38**, 406–416.

2 A. Tlili, F. Monnier and M. Taillefer, *Chem. – A Eur. J.*, 2010, **16**, 12299–12302.

3 S. A. Saucedo Anaya, A. Hagenbach and U. Abram, *Polyhedron*, 2008, **27**, 3587–3592.

4 Y. Yuan, I. Thomé, S. H. Kim, D. Chen, A. Beyer, J. Bonnamour, E. Zuidema, S. Chang and C. Bolm, *Adv. Synth. Catal.*, 2010, **352**, 2892–2898.

5 C. Chachaty, G. C. Pappalardo and G. Scarlata, *J. Chem. Soc. Perkin Trans. 2*, 1976, **23**, 1234.

6 M. Ali, B. Olesen, B. Ranu, L. Clippard, J. Heath, G. Meyer and T. Williams, *Synthesis (Stuttg).*, 2015, **48**, 429–436.

7 C. M. Brown, M. J. Kitt, Z. Xu, D. Hean, M. B. Ezhova and M. O. Wolf, *Inorg. Chem.*, 2017, **56**, 15110–15118.

8 F. Wu, H. Tong, K. Wang, Z. Wang, Z. Li, X. Zhu, W. Y. Wong and W. K. Wong, *J. Photochem. Photobiol. A Chem.*, 2016, **318**, 97–103.

9 C. M. Brown, C. Li, V. Carta, W. Li, Z. Xu, P. H. F. Stroppa, I. D. W. Samuel, E. Zysman-Colman and M. O. Wolf, *Inorg. Chem.*, 2019, **58**, 7156–7168.